# MIMO Channel Shaping and Rate Maximization Using Beyond Diagonal RIS

Yang Zhao, *Member, IEEE,* Hongyu Li, *Member, IEEE,*
Bruno Clerckx, *Fellow, IEEE,* and Massimo Franceschetti, *Fellow, IEEE*

*Abstract*—This paper investigates the limits to which a passive Reconfigurable Intelligent Surface (RIS) can reshape a point-to-point Multiple-Input Multiple-Output (MIMO) in terms of singular values for improved wireless (e.g., rate and power) performance. We depart from the Diagonal (D) scattering matrix and adopt a Beyond Diagonal (BD) model that exploits element-wise connections for signal amplitude and phase manipulation. Specifically, analytical bounds are derived under popular RIS deployment scenarios to showcase the shaping potentials of BD-RIS on the channel Degrees of Freedom (DoF), singular value spread, power gain, and capacity. A numerical optimization method is then proposed for a broader range of shaping problems and invoked to characterize the achievable singular value region. As a side product, we tackle BD-RIS-aided MIMO rate maximization problem by a local-optimal Alternating Optimization (AO) and a low-complexity shaping-inspired approach. Results show that BD-RIS significantly improves the dynamic range of all channel singular values and the trade-off in manipulating them, resulting in enhanced power gain and achievable rate. Those benefits become more pronounced when the number of RIS elements or MIMO dimensions increase. Of particular interest, BD-RIS is shown to activate multi-stream transmission (hence achieving the asymptotic DoF) at much lower transmit power than D-RIS thanks to its singular value shaping proficiency.

*Index Terms*—MIMO, RIS, channel shaping, rate maximization, singular value analysis, manifold optimization.

## I. INTRODUCTION

Today we are witnessing a paradigm shift from connectivity to intelligence, where the wireless environment is no longer a chaotic medium but a conscious agent that can serve on demand. This is empowered by recent advances in Reconfigurable Intelligent Surface (RIS), a programmable passive planar surface that recycles and redistributes ambient electromagnetic waves for improved wireless performance. A typical RIS consists of numerous low-power sub-wavelength non-resonant scattering elements, whose response can be engineered in real-time to manipulate the amplitude, phase, frequency, and polarization of the scattered waves [1]. It enables low-noise full-duplex operation, featuring better flexibility than reflectarrays, lighter footprint

Yang Zhao is with the School of Electronic and Electrical Engineering, University of Leeds, Leeds LS2 9JT, U.K. (email: yang.zhao@ieee.org).

Hongyu Li is with the Internet of Things Thrust, The Hong Kong University of Science and Technology (Guangzhou), Guangdong 511400, P.R. China (email: hongyuli@hkust-gz.edu.cn).

Bruno Clerckx is with the Department of Electrical and Electronic Engineering, Imperial College London, London SW7 2AZ, U.K. (email: b.clerckx@imperial.ac.uk).

Massimo Franceschetti is with the Department of Electrical and Computer Engineering, University of California, San Diego, La Jolla CA 92093, USA (email: massimo@ece.ucsd.edu).

than relays, and greater scalability than Multiple-Input Multiple-Output (MIMO) systems. One popular RIS research direction is *joint passive and active beamforming* design with transceivers to enhance a specific performance measure, which has attracted significant interests in wireless communication [2]–[4], sensing [5]–[7], and power transfer literature [8]–[10]. While passive beamforming at RIS suffers attenuation from double fading, it offers better asymptotic behaviors than active beamforming at transceivers (e.g., second-order array gain and fourth-order harvested power [10]). Another RIS application is *information modulation* by periodically switching its reflection pattern within the channel coherence time. This creates a free-ride message stream with dual benefits: integrating with legacy transmitter for enhanced channel capacity [11], [12], or serving as individual source for low-power uplink communication [13], [14]. Different from above, *channel shaping* exploits RIS as a stand-alone device to modify the inherent properties of the wireless environment, for example, compensate for the Doppler effect [15], flatten frequency-selective channels [16], improve MIMO channel rank [17], and artificially diversify channel over time for orthogonal [18] and non-orthogonal [19] multiple access schemes. This helps to decouple joint beamforming problems into a channel shaping stage and a conventional transceiver design stage, providing a versatile solution for various wireless applications.

At a specific resource block, channel shaping metrics can be classified into two categories.

- *Singular value:* The impact of RIS has been studied in terms of minimum singular value [20], effective rank [21], condition number [22], and Degrees of Freedom (DoF) [23]. Those are closely related to performance measures (e.g., achievable rate and harvested power [24]) but sensitive to minor perturbations of the channel matrix;
- *Power:* The impact of RIS has been studied in terms of channel power gain [2], [25]–[28] in point-to-point channels and leakage interference [29] in interference channels. Those second-order metrics are less informative in MIMO but easier to analyze and optimize.

Although above works offered inspiring glimpses into the channel shaping potential of passive RIS, none attempted to disclose the entire achievable singular value region. Most relevant literature [2], [20]–[23], [29] have also been limited to a Diagonal (D)-RIS model where each element is connected to a dedicated impedance and disconnected from others. As such, wave impinging on one element is entirely scattered by the same element. This architecture is modeled by a diagonal scattering matrix with unit-magnitude diagonal entries, which only applies

a phase shift to the incoming signal under ideal conditions. The concept was later generalized to Beyond Diagonal (BD)-RIS with group-connected architecture [25], where adjacent elements within the same group are connected via passive reconfigurable components, which can be either symmetric (e.g., capacitors and inductors) or asymmetric (e.g., ring hybrids and branch-line hybrids) [30]. This allows wave impinging on one element to propagate within the circuit and depart partially from any element in the same group. It can thus manipulate both amplitude and phase of the scattered wave while remaining passive. Such a powerful model can be realized at reduced hardware cost using tree- and forest-connected architectures by graph theory [27]. BD-RIS can also function in multi-sector mode [31] for full-space coverage and multi-user support. Practical challenges such as channel estimation [32], mutual coupling [33], and wideband modelling [34] have also been studied in recent literature. Its beamforming effectiveness over D-RIS and energy efficiency over active RIS and relay systems have been proved in Single-Input Single-Output (SISO) and Multiple-Input Single-Output (MISO) equivalent systems [25], [27], [28], [31], [35], [36]. However, the interplay between BD-RIS and MIMO is still in the infancy stage. The authors of [37] investigated the rate-optimal joint beamforming design for a fully-connected BD-RIS-aided MIMO system where the direct channel is negligible. A transmitter-side BD-RIS was introduced to massive MIMO systems that exploits statistical Channel State Information (CSI) for improved spectral efficiency [38], which again assumed negligible direct channel and fully-connected BD-RIS. Received power maximization with continuous-valued and discrete-valued BD-RIS have been tackled respectively in closed form [26] and by machine learning approach [39], but the corresponding single-stream transceiver is rate-suboptimal.

This paper is motivated by a fundamental question: *What is the channel shaping capability (in terms of singular values and their functions) of a passive RIS in MIMO channels?* Unlike existing works that focus on specific metrics or scenarios, we aim to develop a broader understanding of RIS in wireless environment manipulation to provide insights for various wireless applications. The contributions are summarized below.

First, we pioneer BD-RIS study in general MIMO channels and interpret its shaping potential as branch matching and mode alignment. Branch matching refers to pairing and combining the branches (i.e., entries) of backward and forward channels associated with each BD-RIS group. Mode alignment refers to aligning and ordering the modes (i.e., singular vectors) of indirect channels with those of direct channel. The former origins uniquely from the off-diagonal entries of the scattering matrix of BD-RIS.

Second, we provide an analytical answer to the shaping question under specific channel conditions. It is shown that BD-RIS may achieve a larger or smaller communication DoF than D-RIS. When the backward or forward channel is rank-deficient, we derive asymptotic bounds of individual singular values applying to D- and BD-RIS. When the direct channel is negligible, we recast the shaping question for fully-connected BD-RIS as a well-studied linear algebra question and provide tight bounds (with closed-form RIS expressions) on channel singular values, power gain, and capacity. These results help to understand the fundamental limits of channel shaping and serve as a foundation for advanced RIS designs.

Third, we provide a numerical answer to the shaping question by exploiting a geodesic Riemannian Conjugate Gradient (RCG) method to optimize the BD-RIS for a broad class of singular value functions. It compares favorably to legacy RIS designs in that the updates are performed multiplicatively along the shortest paths on the manifold for accelerated convergence. The method is then invoked in a Pareto problem to reveal the entire achievable singular value region, which generalizes most relevant metrics and provides an intuitive shaping benchmark.

Fourth, we tackle BD-RIS-aided MIMO rate maximization problem by a local-optimal Alternating Optimization (AO) and a low-complexity shaping-inspired approach. The former iteratively updates the passive beamforming by geodesic RCG and the active beamforming by eigenmode transmission, until convergence. The latter shapes the channel with RIS for maximum power gain and then performs conventional precoding.

Fifth, we conduct extensive simulations to validate the analytical bounds and numerical methods. It is concluded that:

- BD-RIS significantly improves the dynamic range of all channel singular values and the trade-off in manipulating them, resulting in enhanced power gain and achievable rate;
- The shaping benefits of BD-RIS over D-RIS increase with the number of scattering elements, group size, and MIMO dimensions;
- A fully-connected BD-RIS may be designed in closed-form for simultaneous optimality of communication and power transfer;
- BD-RIS can activate multi-stream transmission (hence achieving the asymptotic DoF) at low transmit power thanks to its singular value shaping proficiency;
- The rate gap between the optimal and low-complexity beamforming designs diminishes as the RIS evolves from D to fully-connected BD;
- The additional optimization cost of BD-RIS over D-RIS is affordable and the geodesic RCG method is efficient on large-scale problems;
- The proposed asymmetric RIS designs are robust to channel estimation errors and can be modified for symmetry with reasonable performance cost.

*Notation:* Italic, bold lower-case, and bold upper-case letters indicate scalars, vectors and matrices, respectively. $\jmath$ denotes the imaginary unit. $\mathbb{R}$ and $\mathbb{C}$ denote the set of real and complex numbers, respectively. $\mathbb{H}^{n \times n}$, $\mathbb{H}_+^{n \times n}$, $\mathbb{U}^{n \times n}$, and $\mathbb{P}^{n \times n}$ denote the set of $n \times n$ Hermitian, positive semi-definite, unitary, and permutation matrices, respectively. $\mathbf{0}$ and $\mathbf{I}$ are the zero and identity matrices with appropriate size, respectively. $\Re\{\cdot\}$ takes the real part of a complex number. $\mathbb{E}\{\cdot\}$ is the expectation operator. $\mathrm{tr}(\cdot)$ and $\det(\cdot)$ evaluate the trace and determinant of a square matrix, respectively. $\mathrm{diag}(\cdot)$ constructs a square matrix with arguments on the main (block) diagonal and zeros elsewhere. $\mathrm{sv}(\cdot)$, $\mathrm{ran}(\cdot)$, and $\mathrm{ker}(\cdot)$ evaluate the singular values (in descending order), range, and kernel of a matrix, respectively. $\mathrm{conv}(\cdot)$ returns the convex hull of arguments. $\mathrm{vec}(\cdot)$ stacks the columns of a matrix as a vector. $|\cdot|$, $\|\cdot\|$, and $\|\cdot\|_{\mathrm{F}}$ denote the absolute value, Euclidean norm, and Frobenius norm, respectively. $\sigma_n(\cdot)$ and $\lambda_n(\cdot)$ are the $n$-th

largest singular value and eigenvalue, respectively. $(\cdot)^*$, $(\cdot)^\mathsf{T}$, $(\cdot)^\mathsf{H}$, $(\cdot)^\dagger$, $(\cdot)^\star$ denote the conjugate, transpose, conjugate transpose (Hermitian), Moore-Penrose inverse, and stationary point, respectively. $[N]$ is a shortcut for $\{1,2,...,N\}$. $(\cdot)_{[x:y]}$ is a shortcut for $(\cdot)_x,(\cdot)_{x+1},...,(\cdot)_y$. $\odot$ denotes the Hadamard product. $\mathcal{O}(\cdot)$ is the big-O notation. $\mathcal{N}_\mathbb{C}(\mathbf{0},\boldsymbol{\Sigma})$ is the multivariate Circularly Symmetric Complex Gaussian (CSCG) distribution with mean $\mathbf{0}$ and covariance $\boldsymbol{\Sigma}$. $\sim$ means "distributed as".

## II. System Model

The BD-RIS is modeled as an $N_\mathrm{S}$-port network that divides into $G$ individual groups, where group $g \in [G]$ contains $N_g$ scattering elements interconnected by real-time reconfigurable components [25] satisfying $N_\mathrm{S} = \sum_{g=1}^{G} N_g$. For the ease of analysis, we assume no mutual coupling and equal group size $N_g = L \triangleq N_\mathrm{S}/G$, $\forall g$. The overall scattering matrix of an asymmetric BD-RIS is block-diagonal

$$\boldsymbol{\Theta} = \mathrm{diag}(\boldsymbol{\Theta}_1,...,\boldsymbol{\Theta}_G), \tag{1}$$

where $\boldsymbol{\Theta}_g \in \mathbb{U}^{L \times L}$ is the $g$-th unitary block modeling the response of group $g$. Apparently, D-RIS is an extreme case of (1) with group size $L = 1$. Some viable architectures of BD-RIS are illustrated in [25, Fig. 3], [31, Fig. 5], [27, Fig. 2] where the circuit topology have been modeled in the scattering matrix.

Consider a BD-RIS-aided MIMO point-to-point channel with $N_\mathrm{T}$ and $N_\mathrm{R}$ transmit and receive antennas, respectively, and $N_\mathrm{S}$ scattering elements at the BD-RIS. This configuration is denoted as $N_\mathrm{T} \times N_\mathrm{S} \times N_\mathrm{R}$. Let $\mathbf{H}_\mathrm{D} \in \mathbb{C}^{N_\mathrm{R} \times N_\mathrm{T}}$, $\mathbf{H}_\mathrm{B} \in \mathbb{C}^{N_\mathrm{R} \times N_\mathrm{S}}$, $\mathbf{H}_\mathrm{F} \in \mathbb{C}^{N_\mathrm{S} \times N_\mathrm{T}}$ denote the direct (i.e., transmitter-receiver), backward (i.e., RIS-receiver), and forward (i.e., transmitter-RIS) channels, respectively. The equivalent channel is

$$\mathbf{H} = \mathbf{H}_\mathrm{D} + \mathbf{H}_\mathrm{B}\boldsymbol{\Theta}\mathbf{H}_\mathrm{F} = \mathbf{H}_\mathrm{D} + \sum_g \mathbf{H}_{\mathrm{B},g}\boldsymbol{\Theta}_g\mathbf{H}_{\mathrm{F},g}, \tag{2}$$

where $\mathbf{H}_{\mathrm{B},g} \in \mathbb{C}^{N_\mathrm{R} \times L}$ and $\mathbf{H}_{\mathrm{F},g} \in \mathbb{C}^{L \times N_\mathrm{T}}$ are the backward and forward channels associated with group $g$, corresponding to the $(g-1)L+1$ to $gL$ columns of $\mathbf{H}_\mathrm{B}$ and rows of $\mathbf{H}_\mathrm{F}$, respectively. Since unitary matrices constitute an algebraic group with respect to multiplication, we can decompose the scattering matrix of group $g$ as

$$\boldsymbol{\Theta}_g = \mathbf{L}_g \mathbf{X}_g \mathbf{R}_g^\mathsf{H}, \tag{3}$$

where $\mathbf{L}_g, \mathbf{R}_g \in \mathbb{U}^{L \times L}$ are two unitary matrices and $\mathbf{X}_g \in \mathbb{P}^{n \times n}$ is a permutation matrix. Let $\mathbf{H}_g \triangleq \mathbf{H}_{\mathrm{B},g}\boldsymbol{\Theta}_g\mathbf{H}_{\mathrm{F},g}$ be the indirect channel via group $g$ and $\mathbf{H}_{\mathrm{B/F},g} = \mathbf{U}_{\mathrm{B/F},g}\boldsymbol{\Sigma}_{\mathrm{B/F},g}\mathbf{V}_{\mathrm{B/F},g}^\mathsf{H}$ be the Singular Value Decomposition (SVD) of the backward and forward channels, respectively. The equivalent channel is

$$\mathbf{H} = \overbrace{\mathbf{H}_\mathrm{D} + \sum_g \mathbf{U}_{\mathrm{B},g}\boldsymbol{\Sigma}_{\mathrm{B},g}\underbrace{\mathbf{V}_{\mathrm{B},g}^\mathsf{H}\mathbf{L}_g\mathbf{X}_g\mathbf{R}_g^\mathsf{H}\mathbf{U}_{\mathrm{F},g}}_{\text{backward-forward}}\boldsymbol{\Sigma}_{\mathrm{F},g}\mathbf{V}_{\mathrm{F},g}^\mathsf{H}}^{\text{direct-indirect}}. \tag{4}$$

**Remark 1.** In (4), the BD-RIS performs a blockwise unitary transformation to combine the backward-forward (intra-group, multiplicative) channels and direct-indirect (inter-group, additive) channels. These two attributes are refined respectively as:

- *Branch matching:* To pair and combine the branches (i.e., entries) of $\mathbf{H}_{\mathrm{B},g}$ and $\mathbf{H}_{\mathrm{F},g}$ through $\boldsymbol{\Theta}_g$;

- *Mode alignment:* To align and order the modes (i.e., singular vectors) of $\{\mathbf{H}_g\}_{g \in [G]}$ with those of $\mathbf{H}_\mathrm{D}$ through $\boldsymbol{\Theta}$.

**Example 1** (SISO channel gain maximization). Denote the direct, backward, forward channels as $h_\mathrm{D}$, $\mathbf{h}_\mathrm{B} \in \mathbb{C}^{N_\mathrm{S} \times 1}$, and $\mathbf{h}_\mathrm{F}^\mathsf{H} \in \mathbb{C}^{1 \times N_\mathrm{S}}$, respectively. In this case, mode alignment boils down to phase matching and the optimal BD-RIS structure is

$$\boldsymbol{\Theta}_{\mathrm{P-max},g}^\mathrm{SISO} = \frac{h_\mathrm{D}}{|h_\mathrm{D}|}\mathbf{V}_{\mathrm{B},g}\mathbf{U}_{\mathrm{F},g}^\mathsf{H}, \quad \forall g, \tag{5}$$

where $\mathbf{V}_{\mathrm{B},g} = [\mathbf{h}_{\mathrm{B},g}/\|\mathbf{h}_{\mathrm{B},g}\|, \ \mathbf{N}_{\mathrm{B},g}] \in \mathbb{U}^{L \times L}$, $\mathbf{U}_{\mathrm{F},g} = [\mathbf{h}_{\mathrm{F},g}/\|\mathbf{h}_{\mathrm{F},g}\|, \mathbf{N}_{\mathrm{F},g}] \in \mathbb{U}^{L \times L}$, and $\mathbf{N}_{\mathrm{B/F},g} \in \mathbb{C}^{L \times (L-1)}$ are the orthonormal bases of kernels of $\mathbf{h}_{\mathrm{B/F},g}$. It is evident that any group size $L$ (including D-RIS where the kernels become empty) suffices for perfect phase matching. In contrast, the resulting maximum channel gain still depends on $L$

$$|h| = |h_\mathrm{D}| + \sum_g \sum_l |h_{\mathrm{B},g,\pi_{\mathrm{B},g}(l)}||h_{\mathrm{F},g,\pi_{\mathrm{F},g}(l)}|, \tag{6}$$

where $h_{\mathrm{B/F},g,l}$ are the $l$-th entries of $\mathbf{h}_{\mathrm{B/F},g}$, and $\pi_{\mathrm{B/F},g}$ are permutations of $[L]$ sorting their magnitude in similar orders. That is, the maximum SISO channel gain is attained when each BD-RIS group, apart from phase shifting, matches the $l$-th strongest backward and forward channel branches. A larger $L$ provides more flexible branch matching and thus higher channel gain.

Example 1 clarifies the difference between branch matching and mode alignment and show their impacts on channel shaping. When it comes to MIMO, the advantage of BD-RIS in branch matching improves since the number of available branches is proportional to $N_\mathrm{T}N_\mathrm{R}$. On the other hand, the limitation of D-RIS in mode alignment intensifies since each element can only apply a scalar phase shift to the indirect channel of $N \triangleq \min(N_\mathrm{T},N_\mathrm{S},N_\mathrm{R})$ modes.

## III. Channel Shaping

In this section, we first provide an example demonstrating the MIMO channel shaping advantages of BD-RIS over D-RIS, then derive some analytical bounds on channel singular values and their functions (with closed-form BD-RIS solution) under specific channel conditions. Finally, we propose a numerical method to optimize the BD-RIS for a class of singular value functions under general channel conditions.

**Example 2** ($2 \times 2 \times 2$ shaping). Here D-RIS and fully-connected BD-RIS can be modeled by 2 and 4 independent angular parameters, respectively:

$$\boldsymbol{\Theta}_\mathrm{D} = \mathrm{diag}(e^{\jmath\theta_1},e^{\jmath\theta_2}), \quad \boldsymbol{\Theta}_\mathrm{BD} = e^{\jmath\phi}\begin{bmatrix} e^{\jmath\alpha}\cos\psi & e^{\jmath\beta}\sin\psi \\ -e^{-\jmath\beta}\sin\psi & e^{-\jmath\alpha}\cos\psi \end{bmatrix},$$

We consider a special case where the BD-RIS is symmetric (i.e., $\beta = \pi/2$) and the direct channel is negligible such that $\phi$ has no impact on $\mathrm{sv}(\mathbf{H})$, since $\mathrm{sv}(e^{\jmath\phi}\mathbf{A}) = \mathrm{sv}(\mathbf{A})$. The singular value shaping capabilities of $\boldsymbol{\Theta}_\mathrm{D}$ and $\boldsymbol{\Theta}_\mathrm{BD}$ can thus be compared visually over 2 tunable parameters. With an exhaustive grid search over $(\theta_1,\theta_2)$ and $(\alpha,\psi)$, Fig. 1 shows the achievable singular values of a specific channel instance $\mathbf{H}_\mathrm{B} = \begin{bmatrix} -0.2059+0.5914\jmath & -0.0909+0.5861\jmath \\ 0.4131+0.2651\jmath & -0.1960+0.4650\jmath \end{bmatrix}$, $\mathbf{H}_\mathrm{F} = $
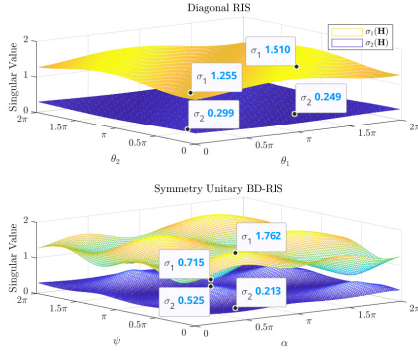
Fig. 1. $2 \times 2 \times 2$ singular value shaping by D-RIS and symmetric fully-connected BD-RIS when the direct channel is negligible. The maximum and minimum of both singular values are marked explicitly on the plot.

$\begin{bmatrix} -0.6362+0.1332\jmath & -0.1572+1.5538\jmath \\ 0.0196+0.4011\jmath & -0.3170-0.2303\jmath \end{bmatrix}$. In this example, both singular values can be manipulated up to[1] $\pm 9\%$ by D-RIS (with 2 reconfigurable components) and $\pm 42\%$ by symmetric fully-connected BD-RIS (with 3 reconfigurable components).

Example 2 suggests that the physical interconnection of RIS elements, even if using symmetric circuit components, can create a "cooperation effect" that significantly enhances the dynamic range of channel singular values. This motivates the analytical and numerical shaping studies in Sections III-A and III-B.

### A. Analytical Shaping Bounds

**Definition 1** (DoF). DoF refers to the maximum number of streams that can be transmitted in parallel over a MIMO channel in the asymptotic high-Signal-to-Noise Ratio (SNR) regime

$$\mathrm{DoF}(\mathbf{H}) = \lim_{\rho \to \infty} \frac{\log\det(\mathbf{I}+\rho\mathbf{H}\mathbf{H}^{\mathsf{H}})}{\log\rho}, \qquad (7)$$

where $\rho$ is the SNR.

**Definition 2** (Negligible direct channel). A direct channel is considered negligible when its contribution to the received signal is substantially weaker than that of the RIS-induced indirect channels. Mathematically, this can be defined as

$$\frac{\|\mathbf{H}_{\mathrm{D}}\|_{\mathrm{F}}^2}{\|\sum_g \mathbf{H}_{\mathrm{B},g}\boldsymbol{\Theta}_g\mathbf{H}_{\mathrm{F},g}\|_{\mathrm{F}}^2} < \epsilon,$$

where $\epsilon$ is a small positive threshold. This can result from a very large number of RIS elements (as in Proposition 2) or physical obstacles in the propagation path (as in Proposition 3).

The main results of this subsection are summarized in the following Propositions and Corollaries.

**Proposition 1** (DoF). *BD-RIS may achieve a larger or smaller MIMO DoF than D-RIS.*

*Proof.* Please refer to Appendix A. □

---

[1]The percentage for manipulating $\sigma_n(\mathbf{H})$ is calculated by $\eta_n^+ = \frac{\max\sigma_n(\mathbf{H})-\mathrm{avg}\sigma_n(\mathbf{H})}{\mathrm{avg}\sigma_n(\mathbf{H})}\times 100\%$ and $\eta_n^- = \frac{\min\sigma_n(\mathbf{H})-\mathrm{avg}\sigma_n(\mathbf{H})}{\mathrm{avg}\sigma_n(\mathbf{H})}\times 100\%$.

While increasing the DoF improves the asymptotic rate performance for point-to-point transmission, the potential to reduce the DoF can be exploited to orthogonalize channels and mitigate interference in multi-user scenarios.

**Example 3** (DoF of $4 \times 4 \times 4$ shaping). Consider a $4 \times 4 \times 4$ shaping with $\mathbf{H}_{\mathrm{D}} = \mathbf{0}$, $\mathbf{H}_{\mathrm{B}} = \begin{bmatrix} 1 & 1 & 0 & 0 \\ 0 & 0 & 0 & 0 \\ 0 & 0 & 1 & 0 \\ 0 & 0 & 0 & 0 \end{bmatrix}$, and $\mathbf{H}_{\mathrm{F}} = \mathrm{diag}(1,1,0,0)$. Evidently, any D-RIS $\boldsymbol{\Theta}_{\mathrm{D}} = \mathrm{diag}(e^{\jmath\theta_1}, e^{\jmath\theta_2}, e^{\jmath\theta_3}, e^{\jmath\theta_4})$ results in

$$\mathbf{H} = \begin{bmatrix} e^{\jmath\theta_1} & e^{\jmath\theta_2} & 0 & 0 \\ 0 & 0 & 0 & 0 \\ 0 & 0 & 0 & 0 \\ 0 & 0 & 0 & 0 \end{bmatrix}$$

with 1 DoF. On the other hand, a fully-connected BD-RIS can perfectly align or misalign the kernels of $\mathbf{H}_{\mathrm{B}}$ and $\mathbf{H}_{\mathrm{F}}$ using the closed-form solutions (46) or (47) in Appendix A. That is,

$$\boldsymbol{\Theta}_{\mathrm{DoF\text{-}max}}^{\mathrm{MIMO}} = \begin{bmatrix} 0 & \frac{1}{\sqrt{2}} & 0 & -\frac{1}{\sqrt{2}} \\ 0 & \frac{1}{\sqrt{2}} & 0 & \frac{1}{\sqrt{2}} \\ -1 & 0 & 0 & 0 \\ 0 & 0 & 1 & 0 \end{bmatrix} \text{ and } \boldsymbol{\Theta}_{\mathrm{DoF\text{-}min}}^{\mathrm{MIMO}} = \begin{bmatrix} -\frac{1}{\sqrt{2}} & 0 & \frac{1}{\sqrt{2}} & 0 \\ \frac{1}{\sqrt{2}} & 0 & \frac{1}{\sqrt{2}} & 0 \\ 0 & 0 & 0 & 1 \\ 0 & -1 & 0 & 0 \end{bmatrix},$$

which correspond to

$$\mathbf{H} = \begin{bmatrix} 0 & \sqrt{2} & 0 & 0 \\ 0 & 0 & 0 & 0 \\ -1 & 0 & 0 & 0 \\ 0 & 0 & 0 & 0 \end{bmatrix}, \quad \mathbf{H} = \mathbf{0},$$

and a DoF of 2 and 0, respectively.

Proposition 1 and Example 3 suggest that we can expect more parallel streams or less interference when shaping the channel with BD-RIS. The latter is particularly helpful in multi-user scenarios where the problem of interest is interference alignment or physical layer security. We now take a step further to examine the limits of redistributing channel singular values under specific channel conditions.

**Proposition 2** (Rank-deficient channel). *If the minimum rank of backward and forward channels is $k$ ($k \leq N$), then for D-RIS or BD-RIS of arbitrary number of elements, the $n$-th singular value of the equivalent channel is bounded above and below respectively by*

$$\sigma_n(\mathbf{H}) \leq \sigma_{n-k}(\mathbf{T}), \qquad \text{if } n > k, \qquad (8a)$$

$$\sigma_n(\mathbf{H}) \geq \sigma_n(\mathbf{T}), \qquad \text{if } n < N-k+1, \qquad (8b)$$

*where $\mathbf{T}$ is any auxiliary matrix satisfying*

$$\mathbf{T}\mathbf{T}^{\mathsf{H}} = \begin{cases} \mathbf{H}_{\mathrm{D}}(\mathbf{I}-\mathbf{V}_{\mathrm{F}}\mathbf{V}_{\mathrm{F}}^{\mathsf{H}})\mathbf{H}_{\mathrm{D}}^{\mathsf{H}}, & \text{if } \mathrm{rank}(\mathbf{H}_{\mathrm{F}}) = k, \\ \mathbf{H}_{\mathrm{D}}^{\mathsf{H}}(\mathbf{I}-\mathbf{U}_{\mathrm{B}}\mathbf{U}_{\mathrm{B}}^{\mathsf{H}})\mathbf{H}_{\mathrm{D}}, & \text{if } \mathrm{rank}(\mathbf{H}_{\mathrm{B}}) = k, \end{cases} \qquad (9)$$

*and $\mathbf{V}_{\mathrm{F}}$ and $\mathbf{U}_{\mathrm{B}}$ are any right and left singular matrices of $\mathbf{H}_{\mathrm{F}}$ and $\mathbf{H}_{\mathrm{B}}$, respectively.*

*Proof.* Please refer to Appendix B. □

Inequality (8a) states that if $\mathbf{H}_{\mathrm{B}}$ and $\mathbf{H}_{\mathrm{F}}$ are at least rank $k$, then with a D-RIS or BD-RIS of *sufficiently large* $N_{\mathrm{S}}$, the $n$-th singular value of $\mathbf{H}$ can be enlarged to the $(n-k)$-th singular value of $\mathbf{T}$, or suppressed to the $n$-th singular value of $\mathbf{T}$. Moreover, the first $k$ channel singular values are unbounded above[2] while the last $k$ channel singular values can be suppressed to zero. A special case of Line-of-Sight (LoS) channel is presented below[3].

---

[2]The energy conservation law $\sum_{n=1}^N \sigma_n^2(\mathbf{H}) \leq 1$ still has to be respected in all cases.

[3]A similar eigenvalue result has been derived for D-RIS only [40].

**Corollary 2.1** (LoS channel). *If at least one of backward and forward channels is LoS, then a D-RIS or BD-RIS can at most enlarge the $n$-th ($n \geq 2$) channel singular value to the $(n-1)$-th singular value of $\mathbf{T}$, or suppress the $n$-th channel singular value to the $n$-th singular value of $\mathbf{T}$. That is,*

$$\sigma_1(\mathbf{H}) \geq \sigma_1(\mathbf{T}) \geq \sigma_2(\mathbf{H}) \geq ... \geq \sigma_{N-1}(\mathbf{T}) \geq \sigma_N(\mathbf{H}) \geq \sigma_N(\mathbf{T}). \tag{10}$$

*Proof.* This is a direct result of (8) with $k=1$. $\qquad\square$

We emphasize that Proposition 2 and Corollary 2.1 apply to both D- and BD-RIS configurations regardless of the status of the direct channel. Out of $2N$ bounds in (8) or (10), $N$ of them can be *simultaneously* tight as $N_S \to \infty$, namely, when the direct channel becomes negligible. For a finite $N_S$, the RIS may prioritize a subset of those by aligning the corresponding modes, and we will later show in Section V that BD-RIS outperforms D-RIS on this purpose. Proposition 2 complements Proposition 1 by quantifying the dynamic range of extreme singular values in low-multipath scenarios and highlights the diminishing returns of increasing $N_S$. Next, we shift the focus to another popular RIS deployment scenario where the direct channel is blocked.

**Proposition 3** (Negligible direct channel). *If the direct channel is negligible, then a fully-connected BD-RIS of arbitrary number of elements can manipulate the channel singular values up to*

$$\mathrm{sv}(\mathbf{H}) = \mathrm{sv}(\mathbf{BF}), \tag{11}$$

*where $\mathbf{B}$ and $\mathbf{F}$ are any matrices satisfying $\mathrm{sv}(\mathbf{B}) = \mathrm{sv}(\mathbf{H}_B)$ and $\mathrm{sv}(\mathbf{F}) = \mathrm{sv}(\mathbf{H}_F)$.*

*Proof.* Please refer to Appendix C. $\qquad\square$

Proposition 3 says that if the direct channel is negligible and the BD-RIS is fully-connected, the only singular value bounds on the equivalent channel are those on the product of unitary-transformed backward and forward channels. It is *not necessarily* an asymptotic result and does *not* depend on any relationship between $N_R$, $N_S$, and $N_T$. Its importance lies in that our initial channel shaping question can be recast as a well-studied linear algebra question: *How the singular values of matrix product are bounded by the singular values of its individual factors?* The question is partially answered in Corollaries 3.1 – 3.3 over the definition $\bar{N} = \max(N_T, N_S, N_R)$ and $\sigma_n(\mathbf{H}) = \sigma_n(\mathbf{H}_F) = \sigma_n(\mathbf{H}_B) = 0$, $\forall n \in [\bar{N}] \setminus [N]$. This is equivalent to padding zero blocks at the end of $\mathbf{H}, \mathbf{H}_B, \mathbf{H}_F$ to make square matrices of dimension $\bar{N}$. The results are by no means complete and interested readers are referred to [41, Chapter 16, 24] and [42, Chapter 3] for more information.

**Corollary 3.1** (Product of subset of singular values). *If the direct channel is negligible, then the product of subset of singular values of $\mathbf{H}$ is bounded from above by those of $\mathbf{H}_B$ and $\mathbf{H}_F$, that is,*

$$\prod_{k \in K} \sigma_k(\mathbf{H}) \leq \prod_{i \in I} \sigma_i(\mathbf{H}_B) \prod_{j \in J} \sigma_j(\mathbf{H}_F), \tag{12}$$

*for all admissible triples $(I,J,K) \in T_r^{\bar{N}}$ with $r < \bar{N}$, where*

$$T_r^{\bar{N}} \triangleq \Big\{ (I,J,K) \in U_r^{\bar{N}} \,\big|\, \forall p < r, \, \forall (F,G,H) \in T_p^r,$$
$$\sum_{f \in F} i_f + \sum_{g \in G} j_g \leq \sum_{h \in H} k_h + \frac{p(p+1)}{2} \Big\},$$
$$U_r^{\bar{N}} \triangleq \Big\{ (I,J,K) \subseteq [\bar{N}]^3 \,\big|\, \sum_{i \in I} i + \sum_{j \in J} j = \sum_{k \in K} k + \frac{r(r+1)}{2} \Big\}.$$

*Proof.* Please refer to [43, Theorem 8]. $\qquad\square$

Inequality (12), also recognized as a variation of Horn's inequality [44], is one of the most comprehensive result over Proposition 3. However, the number of admissible triples increases exponentially[4] with $N_S$ despite some resulting bounds can be redundant. We will shortly see in Corollaries 3.2 and 3.3 that (12) can also induce lower bounds on channel singular values. Those facts render the shaping limit analysis non-trivial for large-scale RIS-aided MIMO systems.

**Corollary 3.2** (Product of some largest or smallest singular values). *If the direct channel is negligible, then the product of the first (resp. last[5]) $k$ singular values of $\mathbf{H}$ is bounded from above (resp. below) by those of $\mathbf{H}_B$ and $\mathbf{H}_F$, that is,*

$$\prod_{n=1}^{k} \sigma_n(\mathbf{H}) \leq \prod_{n=1}^{k} \sigma_n(\mathbf{H}_B) \sigma_n(\mathbf{H}_F), \tag{13a}$$
$$\prod_{n=\bar{N}}^{\bar{N}-k+1} \sigma_n(\mathbf{H}) \geq \prod_{n=\bar{N}}^{\bar{N}-k+1} \sigma_n(\mathbf{H}_B) \sigma_n(\mathbf{H}_F). \tag{13b}$$

*Proof.* Please refer to Appendix D. $\qquad\square$

Corollary 3.2 helps to establish the channel capacity bounds at extreme SNR in Corollary 3.6.

**Corollary 3.3** (Individual singular value). *If the direct channel is negligible, then the $n$-th channel singular value can be manipulated within the range of*

$$\max_{i+j=n+N_S} \sigma_i(\mathbf{H}_B) \sigma_j(\mathbf{H}_F) \leq \sigma_n(\mathbf{H}) \leq \min_{i+j=n+1} \sigma_i(\mathbf{H}_B) \sigma_j(\mathbf{H}_F), \tag{14}$$

*where $(i,j) \in [N_S]^2$. The upper and lower bounds are attained respectively at*

$$\Theta_{\text{sv-}n\text{-max}}^{\text{MIMO-ND}} = \mathbf{V}_B \mathbf{P} \mathbf{U}_F^H, \tag{15a}$$
$$\Theta_{\text{sv-}n\text{-min}}^{\text{MIMO-ND}} = \mathbf{V}_B \mathbf{Q} \mathbf{U}_F^H, \tag{15b}$$

*where $\mathbf{V}_B, \mathbf{U}_F \in \mathbb{U}^{N_S \times N_S}$ are any right and left singular matrices of $\mathbf{H}_B$ and $\mathbf{H}_F$, respectively, and $\mathbf{P}, \mathbf{Q} \in \mathbb{P}^{n \times n}$ are any permutation matrices of dimension $N_S$ satisfying:*

- *The $(i,j)$-th entry is 1, where*

$$(i,j) = \begin{cases} \underset{i+j=n+1}{\arg\min} \, \sigma_i(\mathbf{H}_B) \sigma_j(\mathbf{H}_F) & \text{for } \mathbf{P}, \quad (16a) \\ \underset{i+j=n+N_S}{\arg\max} \, \sigma_i(\mathbf{H}_B) \sigma_j(\mathbf{H}_F) & \text{for } \mathbf{Q}, \quad (16b) \end{cases}$$

*and ties may be broken arbitrarily;*

---

[4]For example, the number of inequalities described by (12) grows from 12 to 2062 when $N_S$ increases from 3 to 7.

[5]The lower bounds coincide at zero when $\bar{N} \neq N$ (i.e., $N_T = N_S = N_R$ being false).

- *After deleting the $i$-th row and $j$-th column, the resulting submatrix $\mathbf{Y} \in \mathbb{P}^{(N_\text{S}-1)\times(N_\text{S}-1)}$ is any permutation matrix satisfying*

$$\sigma_{n-1}(\hat{\mathbf{\Sigma}}_\text{B}\mathbf{Y}\hat{\mathbf{\Sigma}}_\text{F}) \geq \min_{i+j=n+1}\sigma_i(\mathbf{H}_\text{B})\sigma_j(\mathbf{H}_\text{F}) \text{ for } \mathbf{P}, \quad (17\text{a})$$

$$\sigma_{n+1}(\hat{\mathbf{\Sigma}}_\text{B}\mathbf{Y}\hat{\mathbf{\Sigma}}_\text{F}) \leq \max_{i+j=n+N_\text{S}}\sigma_i(\mathbf{H}_\text{B})\sigma_j(\mathbf{H}_\text{F}) \text{ for } \mathbf{Q}, \quad (17\text{b})$$

*where $\hat{\mathbf{\Sigma}}_\text{B}$ and $\hat{\mathbf{\Sigma}}_\text{F}$ are diagonal singular value matrices of $\mathbf{H}_\text{B}$ and $\mathbf{H}_\text{F}$ with both $i$-th row and $j$-th column deleted, respectively.*

*Proof.* Please refer to Appendix E. $\qquad\square$

**Remark 2.** We emphasize that the singular matrices in the SVD are not uniquely defined. When a singular value has multiplicity $k$, the corresponding singular vectors can be any orthonormal basis of the $k$-dimensional subspace. Even if all singular values are distinct, the singular vectors of each can be scaled by a phase factor of choice. Consequently, all SVD-based RIS solutions in this paper are inherently non-unique.

Corollary 3.3 and Proposition 2 both reveal the shaping limits of the $n$-th largest channel singular value, which may be used to simplify the MIMO precoder design with limited number $n$ of Radio Frequency (RF) chains. They are derived under different assumptions are not special cases of each other. Importantly, Corollary 3.3 establishes upper and lower bounds for *each* channel singular value (c.f. first and last $k$ in Proposition 2) and provides general solutions for fully-connected BD-RIS of arbitrary (c.f. sufficiently large) size to attain the equalities. We emphasize that in (15) the mode alignment is realized by $\mathbf{V}_\text{B}$ and $\mathbf{U}_\text{F}$ while the ordering is enabled by permutation matrices $\mathbf{P}$ and $\mathbf{Q}$, which are special cases of $\mathbf{X}$ defined in (3). Specially, the extreme channel singular values can be manipulated within the range of

$$\max_{i+j=N_\text{S}+1}\sigma_i(\mathbf{H}_\text{B})\sigma_j(\mathbf{H}_\text{F}) \leq \sigma_1(\mathbf{H}) \leq \sigma_1(\mathbf{H}_\text{B})\sigma_1(\mathbf{H}_\text{F}), \quad (18\text{a})$$

$$\min_{i+j=\bar{N}+1}\sigma_i(\mathbf{H}_\text{B})\sigma_j(\mathbf{H}_\text{F}) \geq \sigma_{\bar{N}}(\mathbf{H}) \geq \sigma_{\bar{N}}(\mathbf{H}_\text{B})\sigma_{\bar{N}}(\mathbf{H}_\text{F}). \quad (18\text{b})$$

We notice that the right halves in (18a) and (18b) are also special cases of (13a) and (13b) with $k=1$.

**Example 4** (Bounds on $3\times3\times3$ shaping). Consider a $3\times3\times3$ setup with $\mathbf{H}_\text{D}=\mathbf{0}$, $\mathbf{H}_\text{B}=\text{diag}(3,2,1)$, and $\mathbf{H}_\text{F}=\text{diag}(4,0,5)$.
- D-RIS: It is evident that any D-RIS can only achieve $\text{sv}(\mathbf{H}) = [12,5,0]^\mathsf{T}$ due to limited branch matching and mode alignment capabilities;
- BD-RIS: According to (14), a fully-connected BD-RIS can manipulate the singular values within the range of

$$8 \leq \sigma_1(\mathbf{H}) \leq 15, \quad 4 \leq \sigma_2(\mathbf{H}) \leq 10, \quad 0 \leq \sigma_3(\mathbf{H}) \leq 0.$$

To attain the upper and lower bounds, $(i,j)$ in (15a) and (15b) takes $(1,1)$ and $(2,2)$ when $n=1$, and $(2,1)$ and $(3,2)$ when $n=2$, respectively.

We conclude from Example 4 that a fully-connected BD-RIS can widen the dynamic range of channel singular values by properly aligning and ordering the modes of $\mathbf{H}_\text{B}$ and $\mathbf{H}_\text{F}$. However, the individual bounds (14) may not be simultaneously tight when the problem of interest is a function of multiple singular values. Some case studies are presented below.

**Corollary 3.4** (Channel power gain). *If the direct channel is negligible, then the channel power gain is bounded from above (resp. below) by the inner product of squared singular values of $\mathbf{H}_\text{B}$ and $\mathbf{H}_\text{F}$ when they are sorted similarly (resp. oppositely), that is,*

$$\sum_{n=1}^{N}\sigma_n^2(\mathbf{H}_\text{B})\sigma_{N_\text{S}-n+1}^2(\mathbf{H}_\text{F}) \leq \|\mathbf{H}\|_\text{F}^2 \leq \sum_{n=1}^{N}\sigma_n^2(\mathbf{H}_\text{B})\sigma_n^2(\mathbf{H}_\text{F}), \quad (19)$$

*whose upper and lower bounds are attained respectively at*

$$\mathbf{\Theta}_\text{P-max}^\text{MIMO-ND} = \mathbf{V}_\text{B}\mathbf{U}_\text{F}^\mathsf{H}, \quad (20\text{a})$$

$$\mathbf{\Theta}_\text{P-min}^\text{MIMO-ND} = \mathbf{V}_\text{B}\mathbf{J}\mathbf{U}_\text{F}^\mathsf{H}, \quad (20\text{b})$$

*where $\mathbf{J}$ is the exchange (a.k.a. backward identity) matrix of dimension $N_\text{S}$.*

*Proof.* Please refer to Appendix F. $\qquad\square$

We notice that (20a) and (20b) are special cases of (15a) and (15b) with $\mathbf{P}=\mathbf{I}$ and $\mathbf{Q}=\mathbf{J}$, which also attain the right and left halves of (18), respectively. The upper bound (20a) is also reminiscent of the optimal amplify-and-forward relay beamforming design [45, (16), (17)] where the diagonal power allocation matrices boil down to $\mathbf{I}$ due to the passive nature of RIS. As a side note, when both $\mathbf{H}_\text{B}$ and $\mathbf{H}_\text{F}$ follow Rayleigh fading, the expectation of maximum channel power gain can be numerically evaluated as

$$\mathbb{E}\{\|\mathbf{H}\|_\text{F}^2\} = \sum_{n=1}^{N}\iint_0^\infty xy f_{\lambda_n^{\min(N_\text{R},N_\text{S})}}(x) f_{\lambda_n^{\min(N_\text{S},N_\text{T})}}(y)dxdy, \quad (21)$$

where $\lambda_n^K$ is the $n$-th eigenvalue of the complex $K \times K$ Wishart matrix with probability density function $f_{\lambda_n^K}(\cdot)$ given by [46, (51)]. (21) generalizes the SISO channel power gain aided by BD-RIS [25, (58)] to MIMO but a closed-form expression is non-trivial. The next corollary has been derived in [37] independently of Proposition 3 and we include it here for the completeness of results.

**Corollary 3.5** (Channel capacity at general SNR). *If the direct channel is negligible, then the BD-RIS-aided MIMO channel capacity is*

$$C^\text{MIMO-ND} = \sum_{n=1}^{N}\log\left(1+\frac{s_n\sigma_n^2(\mathbf{H}_\text{B})\sigma_n^2(\mathbf{H}_\text{F})}{\eta}\right), \quad (22)$$

*where $\eta$ is the average noise power, $s_n = \mu - \frac{\eta}{\sigma_n^2(\mathbf{H}_\text{B})\sigma_n^2(\mathbf{H}_\text{F})}$ is the power allocated to the $n$-th mode obtainable by the water-filling algorithm [47]. The capacity-achieving BD-RIS scattering matrix is*

$$\mathbf{\Theta}_\text{R-max}^\text{MIMO-ND} = \mathbf{V}_\text{B}\mathbf{U}_\text{F}^\mathsf{H}. \quad (23)$$

*Proof.* Please refer to [37, Appendix A]. $\qquad\square$

Interestingly, the power gain- and rate-optimal scattering matrices (20a) and (23) coincide with each other when the direct channel is negligible and the BD-RIS is fully-connected.

If either condition is false, the active and passive beamforming would be coupled and the rate-optimal solution calls for alternating optimization. The power gain-optimal RIS can still provide a low-complexity decoupled solution and the details will be discussed in Section IV.

**Corollary 3.6** (Channel capacity at extreme SNR)**.** *If the direct channel is negligible, then the channel capacity at extremely low and high SNR $\rho$ are approximately bounded from above by*

$$C_{\rho\downarrow} \lessapprox \rho\sigma_1^2(\mathbf{H}_\mathrm{B})\sigma_1^2(\mathbf{H}_\mathrm{F}), \tag{24a}$$

$$C_{\rho\uparrow} \lessapprox N\log\frac{\rho}{N} + 2\log\prod_{n=1}^{N}\sigma_n(\mathbf{H}_\mathrm{B})\sigma_n(\mathbf{H}_\mathrm{F}). \tag{24b}$$

*Proof.* Please refer to Appendix G. □

The ergodic capacity (22) and (24) when both $\mathbf{H}_\mathrm{B}$ and $\mathbf{H}_\mathrm{F}$ follow Rayleigh fading can be evaluated similarly to (21). Proposition 1 – 3 and the resulting Corollaries provide a partial answer to the channel shaping question in terms of singular values and their functions. Extending the analysis to more general setups and objectives seems non-trivial due to limited branch matching and mode alignment capabilities therein. A numerical solution will be discussed in Section III-B.

*B. Numerical Shaping Solution*

Consider a special class of channel shaping problem

$$\max_{\boldsymbol{\Theta}} \quad f\big(\mathrm{sv}(\mathbf{H})\big) \tag{25a}$$

$$\mathrm{s.t.} \quad \boldsymbol{\Theta}_g^\mathsf{H}\boldsymbol{\Theta}_g = \mathbf{I}, \quad \forall g, \tag{25b}$$

where $f: \mathbb{R}^N \to \mathbb{R}$ is a symmetric gauge function (i.e., a norm invariant under sign change and argument permutation) [48]. Examples of such $f$ include the Ky Fan $k$ norm, Schatten $p$ norm, $n$-th singular value, and channel power gain. Problem (25) is non-convex due to the unitary constraints (25b) and non-smooth due to the possibility of repeated singular values or singular values crossing each other.

**Proposition 4.** *The sub-differential of* (25a) *with respect to BD-RIS block $g$ is*

$$\partial_{\boldsymbol{\Theta}_g^*} f\big(\mathrm{sv}(\mathbf{H})\big) = \mathrm{conv}\big\{\mathbf{H}_{\mathrm{B},g}^\mathsf{H}\mathbf{U}\mathbf{D}\mathbf{V}^\mathsf{H}\mathbf{H}_{\mathrm{F},g}^\mathsf{H}\big\}, \tag{26}$$

*where $\mathbf{D} \in \mathbb{C}^{N_\mathrm{R} \times N_\mathrm{T}}$ is a rectangular diagonal matrix with $[\mathbf{D}]_{n,n} \in \partial_{\sigma_n(\mathbf{H})} f\big(\mathrm{sv}(\mathbf{H})\big), \forall n \in [N]$, and $\mathbf{U}$, $\mathbf{V}$ are any left and right singular matrices of $\mathbf{H}$.*

*Proof.* Please refer to Appendix H. □

With Proposition 4, one can apply the *relax-then-project* method [25], [35] or *non-geodesic*[6] *RCG* [31], [36] to solve problem (25). The former solves unconstrained problem (25a) by quasi-Newton methods and projects the solution back to domain (25b) without optimality guarantee. The latter generalizes the conjugate gradient methods to Riemannian manifolds and updates the solution by addition and retraction, which constitutes a zigzag path departing from and returning to the

---

[6]A geodesic is a curve representing the shortest path between two points in a Riemannian manifold, whose tangent vectors remain parallel when transporting along the curve.

manifold. Next, we introduce a *geodesic RCG* method modified from [49], [50]. Our contribution is an extension to block-unitary cases with sequential, parallel, or unified updates that adapt to and accelerate the design of group-connected BD-RIS.

**Remark 3.** The proposed geodesic RCG method is applicable to a wide range of BD-RIS designs where the objective function is smooth or convex non-smooth and the only constraint is block-unitary scattering matrix.

The steps for updating $\boldsymbol{\Theta}_g$ at iteration $r$ are summarized below, where the gradients can be replaced by sub-gradients for non-smooth $f$.

(i) *Compute the Euclidean gradient at $\boldsymbol{\Theta}_g^{(r)}$:* The gradient of $f$ with respect to $\boldsymbol{\Theta}_g$ in the Euclidean space is

$$\nabla_{\mathrm{E},g}^{(r)} = 2\frac{\partial f(\boldsymbol{\Theta}_g^{(r)})}{\partial \boldsymbol{\Theta}_g^*}; \tag{27}$$

(ii) *Translate to the Riemannian gradient at $\boldsymbol{\Theta}_g^{(r)}$:* At point $\boldsymbol{\Theta}_g^{(r)}$, the Riemannian gradient gives the steepest ascent direction on the manifold. It lies in the tangent space of the manifold $\mathcal{T}_{\boldsymbol{\Theta}_g^{(r)}}\mathbb{U}^{L\times L} \triangleq \{\mathbf{M} \in \mathbb{C}^{L\times L} \mid \mathbf{M}^\mathsf{H}\boldsymbol{\Theta}_g^{(r)} + \boldsymbol{\Theta}_g^{(r)\mathsf{H}}\mathbf{M} = \mathbf{0}\}$ and is obtainable by projection:

$$\nabla_{\mathrm{R},g}^{(r)} = \nabla_{\mathrm{E},g}^{(r)} - \boldsymbol{\Theta}_g^{(r)}\nabla_{\mathrm{E},g}^{(r)\mathsf{H}}\boldsymbol{\Theta}_g^{(r)}; \tag{28}$$

(iii) *Translate to the Riemannian gradient at the identity:* The Riemannian gradient should be translated back to the identity for exploiting the Lie algebra[7]:

$$\tilde{\nabla}_{\mathrm{R},g}^{(r)} = \nabla_{\mathrm{R},g}^{(r)}\boldsymbol{\Theta}_g^{(r)\mathsf{H}} = \nabla_{\mathrm{E},g}^{(r)}\boldsymbol{\Theta}_g^{(r)\mathsf{H}} - \boldsymbol{\Theta}_g^{(r)}\nabla_{\mathrm{E},g}^{(r)\mathsf{H}}. \tag{29}$$

(iv) *Determine the conjugate direction:* The conjugate direction is obtained over the Riemannian gradient and the previous direction as

$$\mathbf{D}_g^{(r)} = \tilde{\nabla}_{\mathrm{R},g}^{(r)} + \gamma_g^{(r)}\mathbf{D}_g^{(r-1)}, \tag{30}$$

where $\gamma_g^{(r)}$ deviates the conjugate direction from the tangent space for accelerated convergence. A popular choice is the Polak-Ribière formula [51]

$$\gamma_g^{(r)} = \frac{\mathrm{tr}\big((\tilde{\nabla}_{\mathrm{R},g}^{(r)} - \tilde{\nabla}_{\mathrm{R},g}^{(r-1)})\tilde{\nabla}_{\mathrm{R},g}^{(r)\mathsf{H}}\big)}{\mathrm{tr}\big(\tilde{\nabla}_{\mathrm{R},g}^{(r-1)}\tilde{\nabla}_{\mathrm{R},g}^{(r-1)\mathsf{H}}\big)}. \tag{31}$$

(v) *Evaluate the geodesic at the identity:* The geodesic emanating from the identity with velocity $\mathbf{D} \in \mathfrak{u}(L)$ is described by

$$\mathbf{G}_\mathbf{I}(\mu) = \exp(\mu\mathbf{D}), \tag{32}$$

where $\exp(\mathbf{A}) = \sum_{k=0}^{\infty}(\mathbf{A}^k/k!)$ is the matrix exponential and $\mu$ is the step size (i.e., magnitude of the tangent vector).

(vi) *Translate to the geodesic at $\boldsymbol{\Theta}_g^{(r)}$:* The geodesic emanating from $\boldsymbol{\Theta}_g^{(r)}$ terminates at $\boldsymbol{\Theta}_g^{(r+1)}$ by multiplicative updates

$$\boldsymbol{\Theta}_g^{(r+1)} = \mathbf{G}_{\boldsymbol{\Theta}_g^{(r)}}(\mu) = \mathbf{G}_\mathbf{I}(\mu)\boldsymbol{\Theta}_g^{(r)} = \exp(\mu\mathbf{D}_g^{(r)})\boldsymbol{\Theta}_g^{(r)}, \tag{33}$$

where $\mu$ is the step size refinable[8] by the Armijo rule [52].

---

[7]Lie algebra refers to the tangent space of the Lie group at the identity element. A Lie group is simultaneously a continuous group and a differentiable manifold. In this example, $\mathbb{U}^{L\times L}$ formulates a Lie group and the corresponding Lie algebra consists of skew-Hermitian matrices $\mathfrak{u}(L) \triangleq \mathcal{T}_\mathbf{I}\mathbb{U}^{L\times L} = \{\mathbf{M} \in \mathbb{C}^{L\times L} \mid \mathbf{M}^\mathsf{H} + \mathbf{M} = \mathbf{0}\}$.

[8]To double the step size, one can simply square the rotation matrix instead of recomputing the matrix exponential, that is, $\exp^2(\mu\mathbf{D}_g^{(r)}) = \exp(2\mu\mathbf{D}_g^{(r)})$.

**Algorithm 1** Geodesic RCG for BD-RIS design

---

**Input:** $f(\boldsymbol{\Theta})$, $G$
**Output:** $\boldsymbol{\Theta}^\star$
1: **Initialize** $r \leftarrow 0$, $\boldsymbol{\Theta}^{(0)}$
2: **Repeat**
3:    **For** $g \leftarrow 1$ to $G$
4:       $\nabla_{\mathrm{E},g}^{(r)} \leftarrow$ (27), $\tilde{\nabla}_{\mathrm{R},g}^{(r)} \leftarrow$ (29), $\gamma_g^{(r)} \leftarrow$ (31), $\mathbf{D}_g^{(r)} \leftarrow$ (30)
5:       **If** $\Re\{\mathrm{tr}(\mathbf{D}_g^{(r)\mathsf{H}}\tilde{\nabla}_{\mathrm{R},g}^{(r)})\} < 0$         ▷ Not ascent
6:         $\mathbf{D}_g^{(r)} \leftarrow \tilde{\nabla}_{\mathrm{R},g}^{(r)}$
7:       **End If**
8:       $\mu \leftarrow 0.1$, $\mathbf{G}_{\boldsymbol{\Theta}_g^{(r)}}(\mu) \leftarrow$ (33)
9:       **While** $f(\mathbf{G}_{\boldsymbol{\Theta}_g^{(r)}}(2\mu)) - f(\boldsymbol{\Theta}_g^{(r)}) \geq \mu \cdot \frac{\mathrm{tr}(\mathbf{D}_g^{(r)}\mathbf{D}_g^{(r)\mathsf{H}})}{2}$
10:         $\mu \leftarrow 2\mu$
11:       **End While**
12:       **While** $f(\mathbf{G}_{\boldsymbol{\Theta}_g^{(r)}}(\mu)) - f(\boldsymbol{\Theta}_g^{(r)}) < \frac{\mu}{2} \cdot \frac{\mathrm{tr}(\mathbf{D}_g^{(r)}\mathbf{D}_g^{(r)\mathsf{H}})}{2}$
13:         $\mu \leftarrow \mu/2$
14:       **End While**
15:       $\boldsymbol{\Theta}_g^{(r+1)} \leftarrow$ (33)
16:    **End For**
17:    $r \leftarrow r+1$
18: **Until** $|f(\boldsymbol{\Theta}^{(r)}) - f(\boldsymbol{\Theta}^{(r-1)})|/f(\boldsymbol{\Theta}^{(r-1)}) \leq \epsilon$

---

Algorithm 1 summarizes the proposed geodesic RCG method with sequential group-wise updates. Compared to the non-geodesic approach, it leverages Lie algebra to replace the add-then-retract update with a multiplicative update (33) along the geodesics of the Stiefel manifold. This appropriate parameter space leads to faster convergence and easier step size tuning. Convergence to a local optimum is still guaranteed if not initialized at a stationary point. The group-wise updates can be performed in parallel to facilitate large-scale BD-RIS design problems. One may directly operate on $\boldsymbol{\Theta}$ and pinching (i.e., keeping the main block diagonal and nulling others) relevant expressions to unify the step size selection for further acceleration.

We now analyze the computational complexity of solving singular value shaping problem (25) by Algorithm 1. To update each BD-RIS group, SVD of $\mathbf{H}$ requires $\mathcal{O}(NN_\mathrm{T}N_\mathrm{R})$ flops, Euclidean sub-gradient (26) requires $\mathcal{O}(LN(N_\mathrm{T}+N_\mathrm{R}+L))$ flops, Riemannian sub-gradient translation (29) requires $\mathcal{O}(L^3)$ flops, deviation parameter (31) and conjugate direction (30) together require $\mathcal{O}(L^2)$ flops, and matrix exponential (33) requires $\mathcal{O}(L^3)$ flops [53]. The overall complexity is thus $\mathcal{O}(I_\mathrm{RCG}G(NN_\mathrm{T}N_\mathrm{R}+LN(N_\mathrm{T}+N_\mathrm{R}+L)+I_\mathrm{BLS}L^3))$, where $I_\mathrm{RCG}$ and $I_\mathrm{BLS}$ are the number of iterations for geodesic RCG and backtracking line search (i.e., lines 9 – 14 of Algorithm 1), respectively. That is, $\mathcal{O}_\mathrm{D}(N_\mathrm{S})$ for D-RIS and $\mathcal{O}_\mathrm{BD}(N_\mathrm{S}^3)$ for fully-connected BD-RIS.

To validate Algorithm 1 and quantify the shaping capability of BD-RIS, we characterize the achievable singular value region of BD-RIS-aided MIMO channel by considering the Pareto optimization problem

$$\max_{\boldsymbol{\Theta}} \quad \sum_{n=1}^{N} \rho_n \sigma_n(\mathbf{H}) \tag{34a}$$
$$\text{s.t.} \quad \boldsymbol{\Theta}_g^\mathsf{H}\boldsymbol{\Theta}_g = \mathbf{I}, \quad \forall g, \tag{34b}$$

where $\rho_n \geq 0$ is the weight associated with the $n$-th channel singular value. Varying those weights help to characterize the Pareto frontier that encloses the achievable singular value region. While the objective (34a) itself seems obscure, a larger quantity translates to a stronger singular value redistribution

capability and thus better wireless performance (e.g., channel capacity for communication [47], detection probability for sensing [54], and harvested power for power transfer [24]). Problem (34) also generalizes the DoF problem in Proposition 1 and the individual singular value shaping problem in Proposition 2 and Corollary 3.3. It can be solved optimally by Algorithm 1 with $[\mathbf{D}]_{n,n} = \rho_n$ in (26).

## IV. RATE MAXIMIZATION

In this section, we first solve the BD-RIS-aided MIMO rate maximization problem optimally by joint beamforming design, and then exploit channel shaping for a low-complexity two-stage solution. The problem is formulated as

$$\max_{\mathbf{W},\boldsymbol{\Theta}} \quad R = \mathrm{logdet}\left(\mathbf{I} + \frac{\mathbf{W}^\mathsf{H}\mathbf{H}^\mathsf{H}\mathbf{H}\mathbf{W}}{\eta}\right) \tag{35a}$$
$$\text{s.t.} \quad \|\mathbf{W}\|_\mathrm{F}^2 \leq P, \tag{35b}$$
$$\boldsymbol{\Theta}_g^\mathsf{H}\boldsymbol{\Theta}_g = \mathbf{I}, \quad \forall g, \tag{35c}$$

where $\mathbf{W}$ is the transmit precoder, $R$ is the achievable rate, $\eta$ is the average noise power, and $P$ is maximum average transmit power. Problem (35) is non-convex due to the block-unitary constraint (35c) and the coupling between variables.

### A. Alternating Optimization

This approach updates $\boldsymbol{\Theta}$ and $\mathbf{W}$ iteratively until convergence. For a given $\mathbf{W}$, the passive beamforming subproblem is

$$\max_{\boldsymbol{\Theta}} \quad \mathrm{logdet}\left(\mathbf{I} + \frac{\mathbf{H}\mathbf{Q}\mathbf{H}^\mathsf{H}}{\eta}\right) \tag{36a}$$
$$\text{s.t.} \quad \boldsymbol{\Theta}_g^\mathsf{H}\boldsymbol{\Theta}_g = \mathbf{I}, \quad \forall g, \tag{36b}$$

where $\mathbf{Q} \triangleq \mathbf{W}\mathbf{W}^\mathsf{H}$ is the transmit covariance matrix. Problem (36) can be solved optimally by Algorithm 1 with the partial derivative given in Lemma 1.

**Lemma 1.** *The partial derivative of* (36a) *with respect to BD-RIS block $g$ is*

$$\frac{\partial R}{\partial \boldsymbol{\Theta}_g^*} = \frac{1}{\eta}\mathbf{H}_{\mathrm{B},g}^\mathsf{H}\left(\mathbf{I} + \frac{\mathbf{H}\mathbf{Q}\mathbf{H}^\mathsf{H}}{\eta}\right)^{-1}\mathbf{H}\mathbf{Q}\mathbf{H}_{\mathrm{F},g}^\mathsf{H}. \tag{37}$$

*Proof.* Please refer to Appendix I. □

For a given $\boldsymbol{\Theta}$, the optimal transmit precoder is given by eigenmode transmission [47]

$$\mathbf{W}^\star = \mathbf{V}\mathrm{diag}(\mathbf{s}^\star)^{1/2}, \tag{38}$$

where $\mathbf{V}$ is the right singular matrix of $\mathbf{H}$ and $\mathbf{s}^\star$ is the optimal water-filling power allocation [47]. The AO algorithm is guaranteed to converge to local-optimal points of problem (35) since each subproblem is solved optimally and the objective is bounded above. The computational complexity of solving subproblem (36) by geodesic RCG is $\mathcal{O}(I_\mathrm{RCG}G(NL^2+LN_\mathrm{T}N_\mathrm{R}+N_\mathrm{T}^2N_\mathrm{R}+N_\mathrm{T}N_\mathrm{R}^2+N_\mathrm{R}^3+I_\mathrm{BLS}L^3))$. On the other hand, the complexity of active beamforming (38) is $\mathcal{O}(NN_\mathrm{T}N_\mathrm{R})$. The overall complexity is thus $\mathcal{O}(I_\mathrm{AO}(I_\mathrm{RCG}G(NL^2+LN_\mathrm{T}N_\mathrm{R}+N_\mathrm{T}^2N_\mathrm{R}+N_\mathrm{T}N_\mathrm{R}^2+N_\mathrm{R}^3+I_\mathrm{BLS}L^3)+NN_\mathrm{T}N_\mathrm{R}))$, where $I_\mathrm{AO}$ is the number of iterations for AO. That is, $\mathcal{O}_\mathrm{D}(N_\mathrm{S})$ for D-RIS and $\mathcal{O}_\mathrm{BD}(N_\mathrm{S}^3)$ for fully-connected BD-RIS.

## B. Low-Complexity Solution

To reduce the computational complexity, we suboptimally decouple the beamforming design by first shape the channel for maximum power gain and then optimize the active beamforming. The shaping subproblem is formulated as

$$\max_{\boldsymbol{\Theta}} \quad \|\mathbf{H}_{\mathrm{D}} + \mathbf{H}_{\mathrm{B}}\boldsymbol{\Theta}\mathbf{H}_{\mathrm{F}}\|_{\mathrm{F}}^2 \tag{39a}$$

$$\text{s.t.} \quad \boldsymbol{\Theta}_g^{\mathsf{H}}\boldsymbol{\Theta}_g = \mathbf{I}, \quad \forall g. \tag{39b}$$

Similar problems have been studied in SISO [25] and MISO equivalents [26], [28], [35], [39] where only one mode is desired. Generalizing those to MIMO is non-trivial due to trade-off between modes. While problem (39) is readily solvable by Algorithm 1, inspired by [55], we further propose a closed-form iterative solution based on orthogonal projection. The idea is to approximate the quadratic objective (39a) successively by Taylor expansion and solve each subproblem by group-wise SVD.

**Proposition 5.** *Starting from any feasible* $\boldsymbol{\Theta}^{(0)}$, *the orthogonal projection of*

$$\mathbf{M}_g^{(r)} = \mathbf{H}_{\mathrm{B},g}^{\mathsf{H}}\Big(\mathbf{H}_{\mathrm{D}} + \mathbf{H}_{\mathrm{B}}\mathrm{diag}\big(\boldsymbol{\Theta}_{[1:g-1]}^{(r+1)}, \boldsymbol{\Theta}_{[g:G]}^{(r)}\big)\mathbf{H}_{\mathrm{F}}\Big)\mathbf{H}_{\mathrm{F},g}^{\mathsf{H}} \tag{40}$$

*onto the Stiefel manifold, given in the closed-form [56]*

$$\boldsymbol{\Theta}_g^{(r+1)} = \operatorname*{argmin}_{\mathbf{X}_g \in \mathbb{U}^{L \times L}} \|\mathbf{M}_g - \mathbf{X}_g\|_{\mathrm{F}} = \mathbf{U}_g^{(r)}\mathbf{V}_g^{(r)\mathsf{H}}, \tag{41}$$

*monotonically increases the objective function* (39a), *where* $\mathbf{U}_g^{(r)}$ *and* $\mathbf{V}_g^{(r)}$ *are any left and right singular matrices of* $\mathbf{M}_g^{(r)}$. *When* (40) *converges,* (41) *leads to a convergence of the objective function* (39a) *towards a stationary point.*

*TODO: power iteration*

*Proof.* Please refer to Appendix J. $\qquad\square$

**Remark 4.** While a rigorous proof remains intricate due to the non-uniqueness of SVD, empirical evidence from extensive simulation indicates that (40) always converge such that (41) always provide an optimal solution.

To update each BD-RIS group, matrix multiplication (40) requires $\mathcal{O}\big(N_{\mathrm{T}}N_{\mathrm{R}} + NL^2 + N_{\mathrm{T}}N_{\mathrm{R}}L\big)$ flops and its SVD requires $\mathcal{O}(L^3)$ flops. The overall complexity is thus $\mathcal{O}\big(I_{\mathrm{SAA}}G\big(N_{\mathrm{T}}N_{\mathrm{R}} + NL^2 + N_{\mathrm{T}}N_{\mathrm{R}}L + L^3\big)\big)$, where $I_{\mathrm{SAA}}$ is the number iterations for successive affine approximation. That is, $\mathcal{O}_{\mathrm{D}}(N_{\mathrm{S}})$ for D-RIS and $\mathcal{O}_{\mathrm{BD}}(N_{\mathrm{S}}^3)$ for fully-connected BD-RIS. For the latter, the computational complexity can be further reduced:

- *Negligible direct channel:* The optimal solution to (39) has been solved in closed form by (20a);
- *Non-negligible direct channel:* In terms of maximizing the inner product $\langle \mathbf{H}_{\mathrm{D}}, \mathbf{H}_{\mathrm{B}}\boldsymbol{\Theta}\mathbf{H}_{\mathrm{F}}\rangle$, (39) is reminiscent of the weighted orthogonal Procrustes problem [57]

$$\min_{\boldsymbol{\Theta}} \quad \|\mathbf{H}_{\mathrm{D}} - \mathbf{H}_{\mathrm{B}}\boldsymbol{\Theta}\mathbf{H}_{\mathrm{F}}\|_{\mathrm{F}}^2 \tag{42a}$$

$$\text{s.t.} \quad \boldsymbol{\Theta}^{\mathsf{H}}\boldsymbol{\Theta} = \mathbf{I}, \tag{42b}$$

which still has no trivial solution. One *lossy* transformation [58] shifts $\boldsymbol{\Theta}$ to sides of the product by Moore-Penrose inverse, formulating standard orthogonal Procrustes problems

$$\min_{\boldsymbol{\Theta}} \quad \|\mathbf{H}_{\mathrm{B}}^{\dagger}\mathbf{H}_{\mathrm{D}} - \boldsymbol{\Theta}\mathbf{H}_{\mathrm{F}}\|_{\mathrm{F}}^2 \text{ or } \|\mathbf{H}_{\mathrm{D}}\mathbf{H}_{\mathrm{F}}^{\dagger} - \mathbf{H}_{\mathrm{B}}\boldsymbol{\Theta}\|_{\mathrm{F}}^2 \tag{43a}$$

TABLE I
PERFORMANCE OF GEODESIC AND NON-GEODESIC RCG ON (34)

| RCG path | $N_{\mathrm{S}} = 16$ | | | $N_{\mathrm{S}} = 256$ | | |
| --- | --- | --- | --- | --- | --- | --- |
| | Objective | Iterations | Time [s] | Objective | Iterations | Time [s] |
| Geodesic | $4.359 \times 10^{-3}$ | 11.59 | $1.839 \times 10^{-2}$ | $1.163 \times 10^{-2}$ | 25.58 | 3.461 |
| Non-geodesic | $4.329 \times 10^{-3}$ | 30.92 | $5.743 \times 10^{-2}$ | $1.116 \times 10^{-2}$ | 61.40 | 13.50 |

TABLE II
PERFORMANCE OF D-RIS AND FULLY-CONNECTED BD-RIS ON (35)

| RIS type | $N_{\mathrm{S}} = 16$ | | | $N_{\mathrm{S}} = 256$ | | |
| --- | --- | --- | --- | --- | --- | --- |
| | Objective | Iterations (outer) | Time [s] | Objective | Iterations (outer) | Time [s] |
| Diagonal | 25.33 | 2.06 | $2.620 \times 10^{-2}$ | 32.22 | 2.92 | 1.277 |
| Fully-connected BD | 26.10 | 3.84 | $2.719 \times 10^{-2}$ | 36.58 | 3.03 | 0.806 |

$$\text{s.t.} \quad \boldsymbol{\Theta}^{\mathsf{H}}\boldsymbol{\Theta} = \mathbf{I}, \tag{43b}$$

with optimal solutions [59, (6.4.1)]

$$\boldsymbol{\Theta}_{\text{P-max-approx}}^{\text{MIMO}} = \mathbf{U}\mathbf{V}^{\mathsf{H}}, \tag{44}$$

where $\mathbf{U}$ and $\mathbf{V}$ are respectively any left and right singular matrices of $\mathbf{H}_{\mathrm{B}}^{\dagger}\mathbf{H}_{\mathrm{D}}\mathbf{H}_{\mathrm{F}}^{\mathsf{H}}$ or $\mathbf{H}_{\mathrm{B}}^{\mathsf{H}}\mathbf{H}_{\mathrm{D}}\mathbf{H}_{\mathrm{F}}^{\dagger}$.

Although (20a) and (44) are of similar form, the latter is neither optimal nor a generalization of the former due to the lossy transformation. We will show in Section V that (44) achieves near-optimal performance. Once the channel is shaped by (41) or (20a) or (44), the active beamforming is retrieved by (38). This two-stage solution avoids outer iterations and efficiently handles (or avoids) inner iterations.

## V. SIMULATION RESULTS

In this section, we provide numerical results to evaluate the proposed BD-RIS designs.[9] Consider a distance-dependent path loss model $\Lambda(d) = \Lambda_0 d^{-\gamma}$ where $\Lambda_0$ is the reference path loss at distance $1\,\mathrm{m}$, $d$ is the propagation distance, and $\gamma$ is the path loss exponent. We set $\Lambda_0 = -30\,\mathrm{dB}$, $\gamma_{\mathrm{D}} = 3$, $\gamma_{\mathrm{F}} = 2.4$, $\gamma_{\mathrm{B}} = 2$, $d_{\mathrm{D}} = 14.7\mathrm{m}$, $d_{\mathrm{F}} = 10\mathrm{m}$, $d_{\mathrm{B}} = 6.3\mathrm{m}$, which corresponds to a typical indoor environment with $\Lambda_{\mathrm{D}} = -65\mathrm{dB}$, $\Lambda_{\mathrm{F}} = -54\mathrm{dB}$, $\Lambda_{\mathrm{B}} = -46\mathrm{dB}$. The small-scale fading model is $\mathbf{H} = \sqrt{\kappa/(1+\kappa)}\mathbf{H}_{\mathrm{LoS}} + \sqrt{1/(1+\kappa)}\mathbf{H}_{\mathrm{NLoS}}$, where $\kappa$ is the Rician K-factor, $\mathbf{H}_{\mathrm{LoS}}$ is the deterministic LoS component, and $\mathbf{H}_{\mathrm{NLoS}} \sim \mathcal{N}_{\mathbb{C}}(\mathbf{0}, \mathbf{I})$ is the Rayleigh component. Unless otherwise specified, we assume the direct channel is present, $\kappa = 0$ (i.e., Rayleigh fading) for all channels, and $\eta = -75\mathrm{dB}$.

### A. Algorithm Evaluation

Table I compares the geodesic RCG method in Algorithm 1 and the non-geodesic RCG method used in [31], [36] on Pareto singular value problem (34) where $N_{\mathrm{T}} = N_{\mathrm{R}} = 4$ and $L = 4$. The statistics are averaged over 100 independent runs. We observe that the geodesic RCG method achieves slightly higher objective values with significantly (down to 1/3) lower number of iterations and shorter (down to 1/4) elapsed time than the non-geodesic method. The results demonstrate the efficiency of the geodesic RCG algorithm 1 on BD-RIS design problems.

---

[9]Source code is available at https://github.com/snowztail/channel-shaping.

(a) $2 \times 32 \times 2$ (no direct)

(b) $2 \times 32 \times 2$

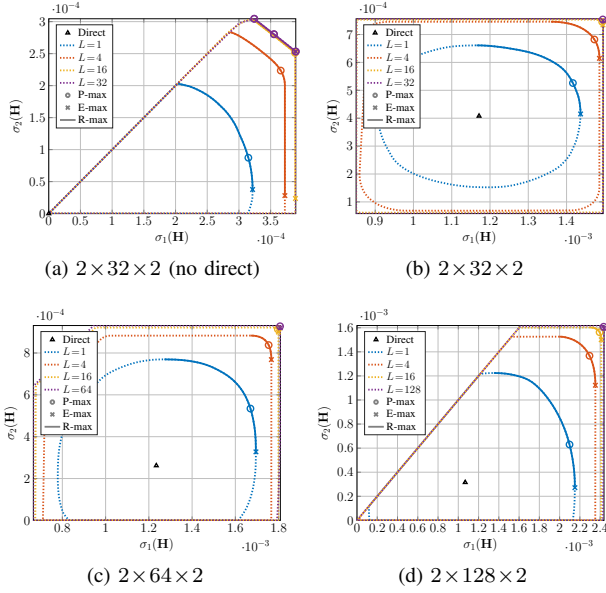(c) $2 \times 64 \times 2$

(d) $2 \times 128 \times 2$

Fig. 2. Achievable singular value regions of an $N_T = N_R = 2$ channel shaped by BD-RIS. The singular value pair of the direct channel are marked as baseline. On the Pareto frontiers, 'P-max', 'E-max', and 'R-max' refer to the channel power gain-optimal point, wireless power transfer-optimal point, and rate-optimal arc, respectively.



(a) $4 \times 32 \times 4$ (rank-1)

(b) $4 \times 64 \times 4$ (rank-1)

(c) $4 \times 128 \times 4$ (rank-2)
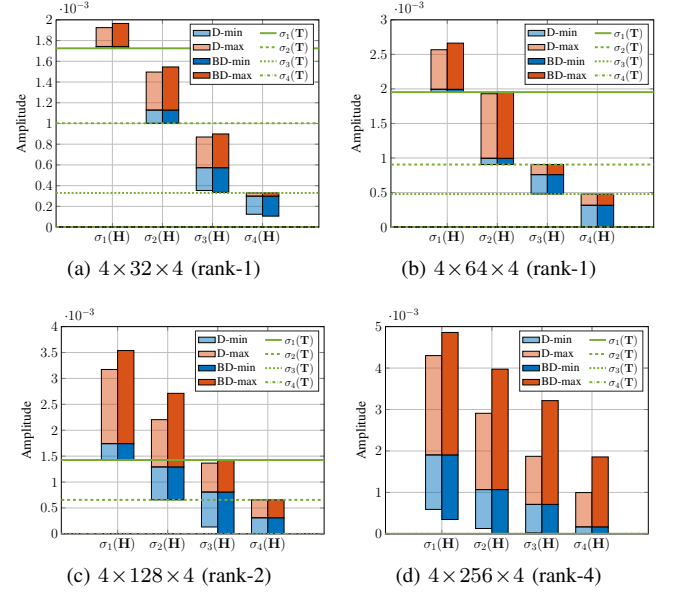
(d) $4 \times 256 \times 4$ (rank-4)

Fig. 3. Achievable channel singular values: analytical bounds (lines) and numerical results (bars). Baselines of bars denote the singular values of the direct channel. Blue (resp. red) bars denote the lower (resp. upper) dynamic range of singular values obtained by solving (34) with $\rho_n / \rho_{n'} \to 0$ (resp. $\to \infty$), $\forall n, \, n' \neq n$. 'D' means D-RIS and 'BD' refers to fully-connected BD-RIS. 'rank-$k$' refers to the rank of the forward channel.

Table II compares the performance of D-RIS and fully-connected BD-RIS on rate maximization problem (35) using the AO design in Section IV-A, where $N_T = N_R = 4$ and $P = 20$dB. The statistics are averaged over 100 independent runs. The fact that fully-connected BD-RIS provides a higher achievable rate using slightly more outer iterations $I_{AO}$ than D-RIS is consistent with our analysis. Interestingly, *the former still ends up with shorter elapsed time,* which seems to contradict the complexity analysis that $\mathcal{O}_{BD}(N_S^3)$ for fully-connected BD-RIS and $\mathcal{O}_D(N_S)$ for D-RIS. One possible reason is that BD-RIS only involves 1 backtracking line search per iteration while D-RIS requires $N_S$ times. Another reason is that the group-wise update of D-RIS leads to slower convergence of inner iterations. These results suggest that optimizing BD-RIS may be less computational intensive than expected.

### B. Channel Singular Value Redistribution

*1) Achievable Singular Value Region:* Fig. 2 illustrates the achievable regions of singular values of an $N_T = N_R = 2$ point-to-point MIMO shaped by RIS, where the channel power gain-optimal point, wireless power transfer-optimal point,[10] and rate-optimal arc are highlighted on the Pareto frontiers. The results are obtained by solving the channel shaping problem (34) merely without any application-specific optimization. As the SNR increases, the rate-optimal point proceeds on the arc from the east (favoring $\sigma_1(\mathbf{H})$) to the north (favoring $\sigma_2(\mathbf{H})$). When the direct channel is negligible, the achievable regions in Fig. 2(a) are shaped like pizza slices. This is because $\sigma_1(\mathbf{H}) \geq \sigma_2(\mathbf{H})$ and there exists a trade-off between the alignment of two modes. The smallest singular value can be

[10] For MIMO wireless power transfer with RF combining, the maximum harvested power depends solely on the dominant channel singular value [24].

enhanced up to $2 \times 10^{-4}$ by D-RIS and $3 \times 10^{-4}$ by fully-connected BD-RIS, corresponding to a $50\%$ gain. We also see that for fully-connected BD-RIS, the power gain-optimal and rate-optimal points coincide as have been proved in (20a) and (23). Interestingly, this observation still holds in Figs. 2(b) – 2(d) where the direct channel is significant, yet a formal proof remains unavailable due to the non-trivial solution structures. The shape of the singular value region depends heavily on the relative strength of the indirect channels, which increases with $N_S$ from the baseline $\Lambda_F \Lambda_B / \Lambda_D = -35$ dB. Fig. 2(b) shows that a 32-element RIS is insufficient to compensate this imbalance and results in a limited singular value region that is symmetric around the direct point. As the group size $L$ increases, the shape of the region evolves from elliptical to square. This transformation not only improves the dynamic range of $\sigma_1(\mathbf{H})$ and $\sigma_2(\mathbf{H})$ by $22\%$ and $38\%$ respectively, but also provides a better trade-off in manipulating both singular values. The observation verifies that the design flexibility of BD-RIS allows better alignment of multiple modes simultaneously. As a consequence, the optimally shaped channels for power gain, communication, and power transfer coincide, implying that a fully-connected BD-RIS may be designed in closed-form for simultaneous multi-functional optimality. The singular value region also enlarges as the number of scattering elements $N_S$ increases. In particular, Fig. 2(d) shows that the equivalent channel can be completely nulled (corresponding to the origin) by a 128-element BD-RIS but not by a diagonal one. The effect may be leveraged for interference cancellation and covert communication. Those results demonstrate the superior channel shaping capability of BD-RIS and emphasizes the importance of adding reconfigurable inter-connections between elements.
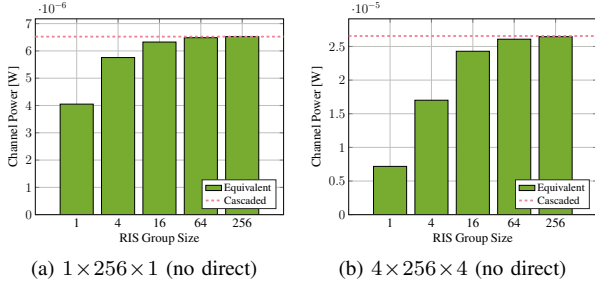
Fig. 4. Average maximum channel power gain versus BD-RIS group size and MIMO dimensions. 'Cascaded' refers to the upper bound in (19).

*2) Analytical Bounds and Numerical Results:* We focus on achieving the asymptotic bounds in Proposition 2 by finite $N_S$, since most results from Proposition 3 are supplied with closed-form RIS solutions. For a rank-$k$ forward channel, Fig. 3 compares the individual singular value bounds in Proposition 2 and the numerical results obtained by solving problem (34) with proper weights. When the RIS is in LoS of the transmitter, Figs. 3(a) and 3(b) show that the achievable channel singular values indeed satisfy Corollary 2.1, namely $\sigma_1(\mathbf{H}) \geq \sigma_1(\mathbf{T})$, $\sigma_2(\mathbf{T}) \leq \sigma_2(\mathbf{H}) \leq \sigma_1(\mathbf{T})$, etc. It is obvious that BD-RIS can approach those bounds better than D-RIS with a small $N_S$. Another example is given in Fig. 3(c) with rank-2 forward channel. The first two channel singular values are unbounded above and bounded below by the first two singular values of $\mathbf{T}$, while the last two singular values can be suppressed to zero and bounded above by the first two singular values of $\mathbf{T}$. Those observations align with Proposition 2. Finally, Fig. 3(d) confirms there are no extra singular value bounds when both backward and forward channels are full-rank. This can be predicted from (9) where $\mathbf{V}_F$ becomes unitary and $\mathbf{T} = \mathbf{0}$. The numerical results are consistent with the analytical bounds, and we conclude that the channel shaping advantage of BD-RIS over D-RIS scales with the rank of backward and forward channels.

Fig. 4 compares the analytical bound on channel power gain in Corollary 3.4 and the numerical results obtained by solving problem (39) when the direct channel is negligible. Here, a fully-connected BD-RIS can attain the upper bound either in closed form (20a) or via optimization approach (41). For the SISO case in Fig. 4(a), the maximum channel power gain is approximately $4 \times 10^{-6}$ by D-RIS and $6.5 \times 10^{-6}$ by fully-connected BD-RIS, corresponding to a $62.5\%$ gain. It comes purely from branch matching as discussed in Example 1 and agrees with the asymptotic power scaling law derived in [25, (30)] Interestingly, Fig. 4(b) shows that this gain surges to $270\%$ in $N_T = N_R = 4$ MIMO and aligns with the expectation analysis (21). We thus conclude that the power gain of BD-RIS scales with group size and MIMO dimensions.

*C. Achievable Rate Maximization*

We first focus on the channel power gain problem (39). Fig. 5 shows the maximum channel power gain under different RIS configurations. An interesting observation is that the relative power gain of BD-RIS over D-RIS is even larger when the direct channel is significant. As shown in Figs. 5(a) and 5(b),
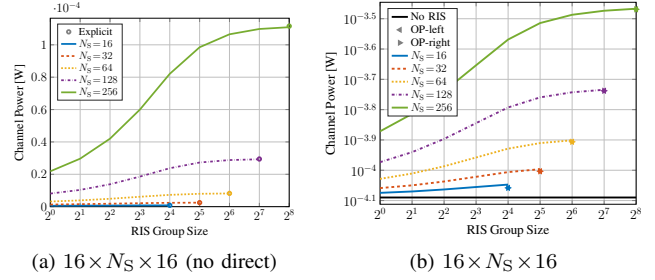


Fig. 5. Average maximum channel power gain versus RIS configuration. 'Explicit' refers to the optimal solution (20a) when the direct channel is negligible. 'OP-left' and 'OP-right' refer to the suboptimal solutions, when the direct channel is significant, by lossy transformation (43) where $\mathbf{\Theta}$ is to the left and right of the product, respectively.
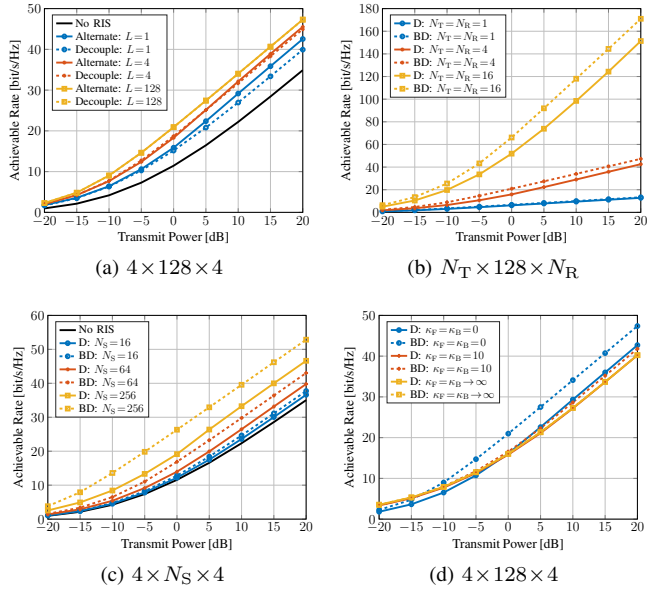


Fig. 6. Average achievable rate versus MIMO and RIS configurations. The transmit power corresponds to a direct SNR of $-10$ to $30$ dB. 'Alternate' refers to the alternating optimization and 'Decouple' refers to the low-complexity design. 'D' means D-RIS and 'BD' refers to fully-connected BD-RIS.

a 64-element fully BD-RIS can almost provide the same channel power gain as a 256-element D-RIS when the direct channel is significant, but less so when it is negligible. This is because the mode alignment advantage of BD-RIS becomes more pronounced when the modes of direct channel is taken into account. We also notice that the suboptimal solutions (44) for fully-connected BD-RIS by lossy transformation (43) are very close to optimal especially for a large $N_S$.

Fig. 6 presents the achievable rate under different MIMO and RIS configurations. At a transmit power $P = 10$dB, Fig. 6(a) shows that introducing a 128-element D-RIS to $N_T = N_R = 4$ MIMO can improve the achievable rate from $22.2$ bps/Hz to $29.2$ bps/Hz $(+31.5\%)$. A BD-RIS of group size 4 and 128 can further elevate those to $32.1$ bps/Hz $(+44.6\%)$ and $34$ bps/Hz $(+53.2\%)$, respectively. An interesting observation is that the rate gap between the optimal AO approach in Section IV-A and the low-complexity shaping-inspired solution in Section IV-B narrows as $L$ increases and completely vanishes for a

(a) Power: $2 \times N_{\mathrm{S}} \times 2$      (b) Rate: $4 \times N_{\mathrm{S}} \times 4$

Fig. 7. Impact of RIS symmetry on the MIMO power gain and achievable rate.



(a) Pareto: $2 \times 64 \times 2$      (b) Rate: $4 \times 128 \times 4$

Fig. 8. Impact of RIS channel estimation error on the MIMO singular value region and achievable rate. A higher transparency of the Pareto frontier indicates a larger channel estimation error. 'D' means D-RIS and 'BD' refers to fully-connected BD-RIS.

fully-connected BD-RIS. This implies that joint beamforming designs may be decoupled by first shaping the wireless channel a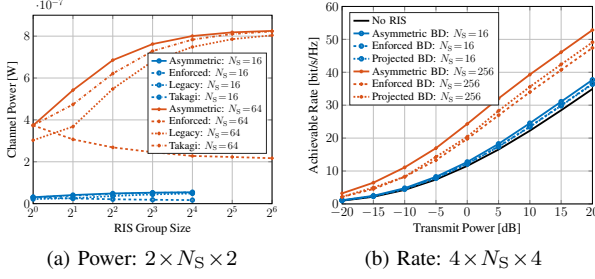nd then optimizing the transmitter, which simplifies the design substantially. Figs. 6(b) and 6(c) also show that both *absolute and relative* rate gains of BD-RIS over D-RIS increases with the number of transmit and receive antennas and scattering elements, especially at high SNR. For $N_{\mathrm{S}} = 128$ and $P = 20$dB, the achievable rate ratio of BD-RIS over D-RIS is 1.04, 1.11, and 1.13 for $N_{\mathrm{T}} = N_{\mathrm{R}} = 1$, 4, and 16, respectively. For $N_{\mathrm{T}} = N_{\mathrm{R}} = 4$ and $P = 20$dB, this ratio amounts to 1.03, 1.08, and 1.13 for $N_{\mathrm{S}} = 16$, 64, and 256, respectively. Those observations align with the power gain results in Fig. 5 and highlight the rate benefits of BD-RIS over D-RIS in large-scale MIMO systems. In the low power regime ($-20$ to $-10$ dB), we also notice that the slope of the achievable rate of BD-RIS is steeper than that of D-RIS. That is, BD-RIS can help to activate more streams and achieve the asymptotic DoF at a low transmit SNR. This is particularly visible in Fig. 6(c) where the topmost curve is almost a linear function of the transmit power. It can be predicted from Fig. 2 that BD-RIS can significantly enlarge all channel singular values for higher receive SNR. Finally, Fig. 6(d) shows that the gap between D- and BD-RIS narrows as the Rician K-factor increases and becomes indistinguishable in LoS environment. The observation is expected from previous studies [25], [26] and aligns with Corollary 2.1, which suggests that the BD-RIS should be deployed in rich-scattering environments to exploit its channel shaping potential.

### D. Practical Constraints

*1) RIS Symmetry:* Symmetric RIS satisfying $\mathbf{\Theta} = \mathbf{\Theta}^{\mathsf{T}}$ are often considered in the literature due to hardware constraints. This study aim to investigate the impact of RIS symmetry on the system performance.

**Remark 5.** All proposed asymmetric BD-RIS designs can be modified for symmetry. In particular,

(i) *SVD-based (e.g., (15), (20), (23), (41), (44)):* Those closed-form asymmetric solutions are constructed from the product of singular matrices. If symmetry is required, one can replace the $\mathbf{U}, \mathbf{V}^{\mathsf{H}}$ in the SVD of $\mathbf{A} = \mathbf{U}\mathbf{\Sigma}\mathbf{V}^{\mathsf{H}}$ by $\mathbf{Q}, \mathbf{Q}^{\mathsf{T}}$ in the Autonne-Takagi factorization of $\frac{\mathbf{A} + \mathbf{A}^{\mathsf{T}}}{2} = \mathbf{Q}\mathbf{\Sigma}\mathbf{Q}^{\mathsf{T}}$ [60] to construct $\mathbf{\Theta}$;

(ii) *RCG-based (e.g., (26), (37)):* The symmetry constraint is added to the corresponding optimization problems, and one can project the solution to the nearest symmetric point $\mathbf{\Theta} \leftarrow \frac{\mathbf{\Theta} + \mathbf{\Theta}^{\mathsf{T}}}{2}$ after each iteration.
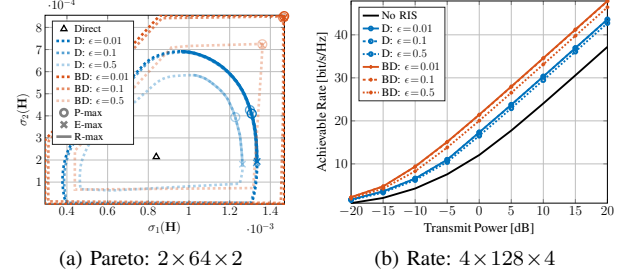
Figs. 7(a) and 7(b) compare the power gain and achievable rate of MIMO point-to-point channel under asymmetric and various symmetric RIS configurations. Here, "asymmetric" refers to the benchmark solution by (41) or (37), "enforced" refers to enforcing symmetry on above, "legacy" refers to a straightforward extension of the SISO SNR-optimal solution [28, (6)], "Takagi" refers to the modification (i), and "projection" refers to the modification (ii). We observe that the performance gaps between the asymmetric and symmetric RIS configurations are insignificant and tends to widen with the number of scattering elements. The two proposed modifications also outperform other candidates in both problems.

*2) Channel Estimation Error:* Figs. 8(a) and 8(b) investigates how RIS channel estimation errors affect the system performance in terms of singular value region and achievable rate. We assume the direct channel can be perfectly acquired and the estimated backward and forward channels are modeled by

$$\hat{\mathbf{H}}_{\mathrm{B/F}} = \mathbf{H}_{\mathrm{B/F}} + \tilde{\mathbf{H}}_{\mathrm{B/F}},$$

where the error follows $\mathrm{vec}(\tilde{\mathbf{H}}_{\mathrm{B/F}}) \sim \mathcal{N}_{\mathbb{C}}(\mathbf{0}, \epsilon \Lambda_{\mathrm{B}} \Lambda_{\mathrm{F}} \mathbf{I})$. The results are evaluated over the ground truth channels. It is observed that the proposed channel shaping and joint beamforming solutions are reasonably robust to channel estimation errors. An interesting observation is that a BD-RIS designed over extremely poorly estimated channels ($\epsilon = 0.5$) may still outpeform a D-RIS designed over almost perfectly estimated channels ($\epsilon = 0.01$). We hope those results can motivate further research on the robust shaping design and provide insights for practical BD-RIS deployment.

### VI. CONCLUSION

This paper analyzes the channel shaping capability of a passive RIS in terms of singular value redistribution. We focus on a BD architecture that allows elements within the same group to interact, enabling more sophisticated manipulation than D-RIS. This translates to a wider dynamic range of and better trade-off between singular values, resulting in significant power and rate gains. Analytical singular value bounds are derived under typical RIS deployment scenarios and the Pareto frontiers are characterized via an efficient RCG method. We also present two beamforming designs for rate maximization problem in MIMO point-to-point channel, one for optimal performance and the other exploits channel shaping for lower

complexity. Extensive simulations show that the shaping advantage of BD-RIS stems from its superior branch matching and mode alignment potentials, which scales with the number of elements, group size, and MIMO dimensions.

## APPENDIX

### A. Proof of Proposition 1

It suffices to consider the rank of the indirect channel. Denote the SVD of the backward and forward channels as

$$\mathbf{H}_{\mathrm{B/F}} = \begin{bmatrix} \mathbf{U}_{\mathrm{B/F},1} & \mathbf{U}_{\mathrm{B/F},2} \end{bmatrix} \begin{bmatrix} \mathbf{\Sigma}_{\mathrm{B/F},1} & \mathbf{0} \\ \mathbf{0} & \mathbf{0} \end{bmatrix} \begin{bmatrix} \mathbf{V}_{\mathrm{B/F},1}^{\mathsf{H}} \\ \mathbf{V}_{\mathrm{B/F},2}^{\mathsf{H}} \end{bmatrix},$$

where $\mathbf{U}_{\mathrm{B/F},1}$ and $\mathbf{V}_{\mathrm{B/F},1}$ are any left and right singular matrices of $\mathbf{H}_{\mathrm{B/F}}$ corresponding to non-zero singular values $\mathbf{\Sigma}_{\mathrm{B/F},1}$, and $\mathbf{U}_{\mathrm{B/F},2}$ and $\mathbf{V}_{\mathrm{B/F},2}$ are those corresponding to zero singular values. The rank of the indirect channel is [41, (16.5.10.b)]

$$\begin{aligned} \mathrm{rank}(\mathbf{H}_{\mathrm{B}}\mathbf{\Theta}\mathbf{H}_{\mathrm{F}}) &= \mathrm{rank}(\mathbf{H}_{\mathrm{B}}) - \dim\bigl(\ker(\mathbf{H}_{\mathrm{F}}^{\mathsf{H}}\mathbf{\Theta}^{\mathsf{H}}) \cap \mathrm{ran}(\mathbf{H}_{\mathrm{B}}^{\mathsf{H}})\bigr) \\ &= \mathrm{rank}(\mathbf{H}_{\mathrm{B}}) - \dim\bigl(\mathrm{ran}(\mathbf{\Theta}\mathbf{U}_{\mathrm{F},2}) \cap \mathrm{ran}(\mathbf{V}_{\mathrm{B},1})\bigr) \\ &\triangleq r_{\mathrm{B}} - r_{\mathrm{L}}(\mathbf{\Theta}), \end{aligned}$$

where we define $r_{\mathrm{L}}(\mathbf{\Theta}) \triangleq \dim\bigl(\mathrm{ran}(\mathbf{\Theta}\mathbf{U}_{\mathrm{F},2}) \cap \mathrm{ran}(\mathbf{V}_{\mathrm{B},1})\bigr)$ and $r_{\mathrm{B/F}} \triangleq \mathrm{rank}(\mathbf{H}_{\mathrm{B/F}})$. Since $\mathbf{U}_{\mathrm{F},2} \in \mathbb{U}^{N_{\mathrm{S}} \times (N_{\mathrm{S}} - r_{\mathrm{F}})}$ and $\mathbf{V}_{\mathrm{B},1} \in \mathbb{U}^{N_{\mathrm{S}} \times r_{\mathrm{B}}}$, we have $\max(r_{\mathrm{B}} - r_{\mathrm{F}}, 0) \le r_{\mathrm{L}}(\mathbf{\Theta}) \le \min(N_{\mathrm{S}} - r_{\mathrm{F}}, r_{\mathrm{B}})$ and thus

$$\max(r_{\mathrm{B}} + r_{\mathrm{F}} - N_{\mathrm{S}}, 0) \le \mathrm{rank}(\mathbf{H}_{\mathrm{B}}\mathbf{\Theta}\mathbf{H}_{\mathrm{F}}) \le \min(r_{\mathrm{B}}, r_{\mathrm{F}}). \quad (45)$$

To attain the upper bound in (45), the RIS needs to minimize $r_{\mathrm{L}}(\mathbf{\Theta})$ by aligning the ranges of $\mathbf{\Theta}\mathbf{U}_{\mathrm{F},2}$ and $\mathbf{V}_{\mathrm{B},2}$ as much as possible. This is achieved by

$$\mathbf{\Theta}_{\mathrm{DoF\text{-}max}}^{\mathrm{MIMO}} = \mathbf{Q}_{\mathrm{B},2}\mathbf{Q}_{\mathrm{F},2}^{\mathsf{H}}, \quad (46)$$

where $\mathbf{Q}_{\mathrm{B},2}$ and $\mathbf{Q}_{\mathrm{F},2}$ are the unitary matrices of the QR decomposition of $\mathbf{V}_{\mathrm{B},2}$ and $\mathbf{U}_{\mathrm{F},2}$, respectively. Similarly, the lower bound in (45) is attained at

$$\mathbf{\Theta}_{\mathrm{DoF\text{-}min}}^{\mathrm{MIMO}} = \mathbf{Q}_{\mathrm{B},1}\mathbf{Q}_{\mathrm{F},2}^{\mathsf{H}}, \quad (47)$$

where $\mathbf{Q}_{\mathrm{B},1}$ is the unitary matrix of the QR decomposition of $\mathbf{V}_{\mathrm{B},1}$. While the DoF-optimal structures (46) and (47) are always feasible for fully-connected BD-RIS, they are generally infeasible for D-RIS unless there exist some QR decomposition that diagonalize $\mathbf{Q}_{\mathrm{B},2}\mathbf{Q}_{\mathrm{F},2}^{\mathsf{H}}$ and $\mathbf{Q}_{\mathrm{B},1}\mathbf{Q}_{\mathrm{F},2}^{\mathsf{H}}$ simultaneously. That is, BD-RIS may achieve a larger or smaller number of DoF of indirect channel, and thus equivalent channel, than D-RIS.

### B. Proof of Proposition 2

We consider rank-$k$ forward channel and the proof follows similarly for rank-$k$ backward channel. Let $\mathbf{H}_{\mathrm{F}} = \mathbf{U}_{\mathrm{F}}\mathbf{\Sigma}_{\mathrm{F}}\mathbf{V}_{\mathrm{F}}^{\mathsf{H}}$ be the SVD of the forward channel. The channel Gram matrix $\mathbf{G} \triangleq \mathbf{H}\mathbf{H}^{\mathsf{H}}$ can be written as

$$\begin{aligned} \mathbf{G} &= \mathbf{H}_{\mathrm{D}}\mathbf{H}_{\mathrm{D}}^{\mathsf{H}} + \mathbf{H}_{\mathrm{B}}\mathbf{\Theta}\mathbf{U}_{\mathrm{F}}\mathbf{\Sigma}_{\mathrm{F}}\mathbf{\Sigma}_{\mathrm{F}}^{\mathsf{H}}\mathbf{U}_{\mathrm{F}}^{\mathsf{H}}\mathbf{\Theta}^{\mathsf{H}}\mathbf{H}_{\mathrm{B}}^{\mathsf{H}} \\ &\quad + \mathbf{H}_{\mathrm{B}}\mathbf{\Theta}\mathbf{U}_{\mathrm{F}}\mathbf{\Sigma}_{\mathrm{F}}\mathbf{V}_{\mathrm{F}}^{\mathsf{H}}\mathbf{H}_{\mathrm{D}}^{\mathsf{H}} + \mathbf{H}_{\mathrm{D}}\mathbf{V}_{\mathrm{F}}\mathbf{\Sigma}_{\mathrm{F}}\mathbf{U}_{\mathrm{F}}^{\mathsf{H}}\mathbf{\Theta}^{\mathsf{H}}\mathbf{H}_{\mathrm{B}}^{\mathsf{H}} \\ &= \mathbf{H}_{\mathrm{D}}(\mathbf{I} - \mathbf{V}_{\mathrm{F}}\mathbf{V}_{\mathrm{F}}^{\mathsf{H}})\mathbf{H}_{\mathrm{D}}^{\mathsf{H}} \\ &\quad + (\mathbf{H}_{\mathrm{B}}\mathbf{\Theta}\mathbf{U}_{\mathrm{F}}\mathbf{\Sigma}_{\mathrm{F}} + \mathbf{H}_{\mathrm{D}}\mathbf{V}_{\mathrm{F}})(\mathbf{\Sigma}_{\mathrm{F}}\mathbf{U}_{\mathrm{F}}^{\mathsf{H}}\mathbf{\Theta}^{\mathsf{H}}\mathbf{H}_{\mathrm{B}}^{\mathsf{H}} + \mathbf{V}_{\mathrm{F}}^{\mathsf{H}}\mathbf{H}_{\mathrm{D}}^{\mathsf{H}}) \\ &= \mathbf{Y} + \mathbf{Z}\mathbf{Z}^{\mathsf{H}}, \end{aligned}$$

where we define $\mathbf{Y} \triangleq \mathbf{H}_{\mathrm{D}}(\mathbf{I} - \mathbf{V}_{\mathrm{F}}\mathbf{V}_{\mathrm{F}}^{\mathsf{H}})\mathbf{H}_{\mathrm{D}}^{\mathsf{H}} \in \mathbb{H}^{N_{\mathrm{R}} \times N_{\mathrm{R}}}$ and $\mathbf{Z} \triangleq \mathbf{H}_{\mathrm{B}}\mathbf{\Theta}\mathbf{U}_{\mathrm{F}}\mathbf{\Sigma}_{\mathrm{F}} + \mathbf{H}_{\mathrm{D}}\mathbf{V}_{\mathrm{F}} \in \mathbb{C}^{N_{\mathrm{R}} \times k}$. That is to say, $\mathbf{G}$ can be expressed as a Hermitian matrix plus $k$ rank-1 perturbations. According to the Cauchy interlacing formula [59, Theorem 8.4.3], the $n$-th eigenvalue of $\mathbf{G}$ is bounded by

$$\lambda_n(\mathbf{G}) \le \lambda_{n-k}(\mathbf{Y}), \qquad \text{if } n > k, \quad (48)$$

$$\lambda_n(\mathbf{G}) \ge \lambda_n(\mathbf{Y}), \qquad \text{if } n < N - k + 1. \quad (49)$$

Since $\mathbf{Y} = \mathbf{T}\mathbf{T}^{\mathsf{H}}$ is positive semi-definite, taking the square roots of (48) and (49) gives (8a) and (8b).

### C. Proof of Proposition 3

Let $\mathbf{H}_{\mathrm{B}} = \mathbf{U}_{\mathrm{B}}\mathbf{\Sigma}_{\mathrm{B}}\mathbf{V}_{\mathrm{B}}^{\mathsf{H}}$ and $\mathbf{H}_{\mathrm{F}} = \mathbf{U}_{\mathrm{F}}\mathbf{\Sigma}_{\mathrm{F}}\mathbf{V}_{\mathrm{F}}^{\mathsf{H}}$ be the SVD of the backward and forward channels, respectively. The scattering matrix of fully-connected BD-RIS can be decomposed as

$$\mathbf{\Theta} = \mathbf{V}_{\mathrm{B}}\mathbf{X}\mathbf{U}_{\mathrm{F}}^{\mathsf{H}}, \quad (50)$$

where $\mathbf{X} \in \mathbb{U}^{N_{\mathrm{S}} \times N_{\mathrm{S}}}$ is a unitary matrix to be designed. The equivalent channel is thus a function of $\mathbf{X}$

$$\mathbf{H} = \mathbf{H}_{\mathrm{B}}\mathbf{\Theta}\mathbf{H}_{\mathrm{F}} = \mathbf{U}_{\mathrm{B}}\mathbf{\Sigma}_{\mathrm{B}}\mathbf{X}\mathbf{\Sigma}_{\mathrm{F}}\mathbf{V}_{\mathrm{F}}^{\mathsf{H}}. \quad (51)$$

Since $\mathrm{sv}(\mathbf{U}\mathbf{A}\mathbf{V}^{\mathsf{H}}) = \mathrm{sv}(\mathbf{A})$ for unitary $\mathbf{U}$ and $\mathbf{V}$, we have

$$\begin{aligned} \mathrm{sv}(\mathbf{H}) &= \mathrm{sv}(\mathbf{U}_{\mathrm{B}}\mathbf{\Sigma}_{\mathrm{B}}\mathbf{X}\mathbf{\Sigma}_{\mathrm{F}}\mathbf{V}_{\mathrm{F}}^{\mathsf{H}}) \\ &= \mathrm{sv}(\mathbf{\Sigma}_{\mathrm{B}}\mathbf{X}\mathbf{\Sigma}_{\mathrm{F}}) \\ &= \mathrm{sv}(\bar{\mathbf{U}}_{\mathrm{B}}\mathbf{\Sigma}_{\mathrm{B}}\bar{\mathbf{V}}_{\mathrm{B}}^{\mathsf{H}}\bar{\mathbf{U}}_{\mathrm{F}}\mathbf{\Sigma}_{\mathrm{F}}\bar{\mathbf{V}}_{\mathrm{F}}^{\mathsf{H}}) \\ &= \mathrm{sv}(\mathbf{B}\mathbf{F}), \end{aligned} \quad (52)$$

where $\bar{\mathbf{U}}_{\mathrm{B}} \in \mathbb{U}^{N_{\mathrm{R}} \times N_{\mathrm{R}}}$, $\bar{\mathbf{V}}_{\mathrm{B}}, \bar{\mathbf{U}}_{\mathrm{F}} \in \mathbb{U}^{N_{\mathrm{S}} \times N_{\mathrm{S}}}$, and $\bar{\mathbf{V}}_{\mathrm{F}} \in \mathbb{U}^{N_{\mathrm{T}} \times N_{\mathrm{T}}}$ can be designed arbitrarily.

### D. Proof of Corollary 3.2

(13a) follows from (12) when $r = k$. On the other hand, if we can prove

$$\prod_{n=1}^{\bar{N}} \sigma_n(\mathbf{H}) = \prod_{n=1}^{\bar{N}} \sigma_n(\mathbf{H}_{\mathrm{B}})\sigma_n(\mathbf{H}_{\mathrm{F}}), \quad (53)$$

then (13b) follows from (13a) and the non-negativity of singular values. To see (53), we start from a stricter result

$$\prod_{n=1}^{N_{\mathrm{S}}} \sigma_n(\mathbf{H}) = \prod_{n=1}^{N_{\mathrm{S}}} \sigma_n(\mathbf{H}_{\mathrm{B}})\sigma_n(\mathbf{H}_{\mathrm{F}}), \quad (54)$$

which is provable by cases. When $N_{\mathrm{S}} > N$, both sides of (54) become zero since $\sigma_n(\mathbf{H}) = \sigma_n(\mathbf{H}_{\mathrm{B}}) = \sigma_n(\mathbf{H}_{\mathrm{F}}) = 0$ for $n > N$. When $N_{\mathrm{S}} \le N$, we have

$$\begin{aligned} \prod_{n=1}^{N_{\mathrm{S}}} \sigma_n(\mathbf{H}) &= \prod_{n=1}^{N_{\mathrm{S}}} \sigma_n(\mathbf{\Sigma}_{\mathrm{B}}\mathbf{X}\mathbf{\Sigma}_{\mathrm{F}}) \\ &= \prod_{n=1}^{N_{\mathrm{S}}} \sigma_n(\hat{\mathbf{\Sigma}}_{\mathrm{B}}\mathbf{X}\hat{\mathbf{\Sigma}}_{\mathrm{F}}) \\ &= \det(\hat{\mathbf{\Sigma}}_{\mathrm{B}}\mathbf{X}\hat{\mathbf{\Sigma}}_{\mathrm{F}}) \\ &= \det(\hat{\mathbf{\Sigma}}_{\mathrm{B}})\det(\mathbf{X})\det(\hat{\mathbf{\Sigma}}_{\mathrm{F}}) \\ &= \prod_{n=1}^{N_{\mathrm{S}}} \sigma_n(\mathbf{\Sigma}_{\mathrm{B}})\sigma_n(\mathbf{\Sigma}_{\mathrm{F}}), \end{aligned}$$

where the first equality follows from (52) and $\hat{\mathbf{\Sigma}}_{\mathrm{B}}, \hat{\mathbf{\Sigma}}_{\mathrm{F}}$ truncate $\mathbf{\Sigma}_{\mathrm{B}}, \mathbf{\Sigma}_{\mathrm{F}}$ to square matrices of dimension $N_{\mathrm{S}}$, respectively. It is evident that (54) implies (53) and thus (13b).

## E. Proof of Corollary 3.3

In (14), the set of upper bounds

$$\big\{\sigma_n(\mathbf{H})\leq\sigma_i(\mathbf{H}_\mathrm{B})\sigma_j(\mathbf{H}_\mathrm{F})\,|\,[i,j,k]\in[N_\mathrm{S}]^3,i+j=n+1\big\} \quad (55)$$

is a special case of (12) with $(I,J,K)\in[N_\mathrm{S}]^3$. The minimum[11] of (55) is selected as the tightest upper bound in (14). On the other hand, the set of lower bounds

$$\big\{\sigma_n(\mathbf{H})\geq\sigma_i(\mathbf{H}_\mathrm{B})\sigma_j(\mathbf{H}_\mathrm{F})\,|\,[i,j,k]\in[N_\mathrm{S}]^3,i+j=n+N_\mathrm{S}\big\} \quad (56)$$

can be induced by (55), (54), and the non-negativity of singular values. The maximum of (56) is selected as the tightest lower bound in (14). Interested readers are also referred to [61, (2.0.3)].

To attain the upper bound, the BD-RIS needs to maximize the minimum of the first $n$ channel singular values. It follows from (15a) that

$$\begin{aligned}\mathrm{sv}(\mathbf{H})&=\mathrm{sv}(\mathbf{H}_\mathrm{B}\mathbf{V}_\mathrm{B}\mathbf{P}\mathbf{U}_\mathrm{F}^\mathsf{H}\mathbf{H}_\mathrm{F})\\&=\mathrm{sv}(\mathbf{U}_\mathrm{B}\boldsymbol{\Sigma}_\mathrm{B}\mathbf{V}_\mathrm{B}^\mathsf{H}\mathbf{V}_\mathrm{B}\mathbf{P}\mathbf{U}_\mathrm{F}^\mathsf{H}\mathbf{U}_\mathrm{F}\boldsymbol{\Sigma}_\mathrm{F}\mathbf{U}_\mathrm{F}^\mathsf{H})\\&=\mathrm{sv}(\boldsymbol{\Sigma}_\mathrm{B}\mathbf{P}\boldsymbol{\Sigma}_\mathrm{F}).\end{aligned}$$

On the one hand, $\mathbf{P}_{ij}=1$ with $(i,j)$ satisfying (16a) ensures $\min_{i+j=n+1}\sigma_i(\mathbf{H}_\mathrm{B})\sigma_j(\mathbf{H}_\mathrm{F})$ is a singular value of $\mathbf{H}$. It is actually among the first $n$ since the number of pairs $(i',j')$ not majorized by $(i,j)$ is $n-1$. On the other hand, (17a) ensures the first $(n-1)$-th singular values are no smaller than $\min_{i+j=n+1}\sigma_i(\mathbf{H}_\mathrm{B})\sigma_j(\mathbf{H}_\mathrm{F})$. Combining both facts, we claim the upper bound $\sigma_n(\mathbf{H})=\min_{i+j=n+1}\sigma_i(\mathbf{H}_\mathrm{B})\sigma_j(\mathbf{H}_\mathrm{F})$ is attainable by (15a). The attainability of the lower bound can be proved similarly and the details are omitted.

## F. Proof of Corollary 3.4

From (50) and (51) we have

$$\begin{aligned}\|\mathbf{H}\|_\mathrm{F}^2&=\mathrm{tr}\big(\mathbf{V}_\mathrm{F}\boldsymbol{\Sigma}_\mathrm{F}^\mathsf{H}\mathbf{X}^\mathsf{H}\boldsymbol{\Sigma}_\mathrm{B}^\mathsf{H}\mathbf{U}_\mathrm{B}^\mathsf{H}\mathbf{U}_\mathrm{B}\boldsymbol{\Sigma}_\mathrm{B}\mathbf{X}\boldsymbol{\Sigma}_\mathrm{F}\mathbf{V}_\mathrm{F}^\mathsf{H}\big)\\&=\mathrm{tr}\big(\boldsymbol{\Sigma}_\mathrm{B}^\mathsf{H}\boldsymbol{\Sigma}_\mathrm{B}\cdot\mathbf{X}\boldsymbol{\Sigma}_\mathrm{F}\boldsymbol{\Sigma}_\mathrm{F}^\mathsf{H}\mathbf{X}^\mathsf{H}\big) \quad (57)\\&\triangleq\mathrm{tr}\big(\tilde{\mathbf{B}}\tilde{\mathbf{F}}\big),\end{aligned}$$

where $\mathbf{X}\triangleq\mathbf{V}_\mathrm{B}^\mathsf{H}\boldsymbol{\Theta}\mathbf{U}_\mathrm{F}\in\mathbb{U}^{N_\mathrm{S}\times N_\mathrm{S}}$, $\tilde{\mathbf{B}}\triangleq\boldsymbol{\Sigma}_\mathrm{B}^\mathsf{H}\boldsymbol{\Sigma}_\mathrm{B}\in\mathbb{H}_+^{N_\mathrm{S}\times N_\mathrm{S}}$, and $\tilde{\mathbf{F}}\triangleq\mathbf{X}\boldsymbol{\Sigma}_\mathrm{F}\boldsymbol{\Sigma}_\mathrm{F}^\mathsf{H}\mathbf{X}^\mathsf{H}\in\mathbb{H}_+^{N_\mathrm{S}\times N_\mathrm{S}}$. By Ruhe's trace inequality for positive semi-definite matrices [62, (H.1.g) and (H.1.h)],

$$\sum_{n=1}^N\lambda_n(\tilde{\mathbf{B}})\lambda_{N_\mathrm{S}-n+1}(\tilde{\mathbf{F}})\leq\mathrm{tr}\big(\tilde{\mathbf{B}}\tilde{\mathbf{F}}\big)\leq\sum_{n=1}^N\lambda_n(\tilde{\mathbf{B}})\lambda_n(\tilde{\mathbf{F}}),$$

which simplifies to (19). The upper bound is attained when $\mathbf{X}$ is chosen to match the singular values of $\tilde{\mathbf{F}}$ to those of $\tilde{\mathbf{B}}$ in similar order. Apparently this occurs at $\mathbf{X}=\mathbf{I}$ and $\boldsymbol{\Theta}=\mathbf{V}_\mathrm{B}\mathbf{U}_\mathrm{F}^\mathsf{H}$. On the other hand, the lower bound is attained when the singular values of $\tilde{\mathbf{F}}$ and $\tilde{\mathbf{B}}$ are matched in reverse order, namely $\mathbf{X}=\mathbf{J}$ and $\boldsymbol{\Theta}=\mathbf{V}_\mathrm{B}\mathbf{J}\mathbf{U}_\mathrm{F}^\mathsf{H}$.

---

[11]One may think to take the maximum of those upper bounds as the problem of interest is the attainable dynamic range of $n$-th singular value. This is infeasible since the singular values will be reordered.

## G. Proof of Corollary 3.6

When perfect CSI is available at the transmitter, in the low-SNR regime, the capacity is achieved by dominant eigenmode transmission [47, (5.26)]

$$\begin{aligned}C_{\rho_\downarrow}&=\log\big(1+\rho\lambda_1(\mathbf{H}^\mathsf{H}\mathbf{H})\big)\\&=\log\big(1+\rho\sigma_1^2(\mathbf{H})\big)\\&\approx\rho\sigma_1^2(\mathbf{H})\\&\leq\rho\sigma_1^2(\mathbf{H}_\mathrm{B})\sigma_1^2(\mathbf{H}_\mathrm{F}),\end{aligned}$$

where the approximation is $\log(1+x)\approx x$ for small $x$ and the inequality follows from (13a) with $k=1$. In the high-SNR regime, the capacity is achieved by multiple eigenmode transmission with uniform power location [47, (5.27)]

$$\begin{aligned}C_{\rho_\uparrow}&=\sum_{n=1}^N\log\Big(1+\frac{\rho}{N}\lambda_n(\mathbf{H}^\mathsf{H}\mathbf{H})\Big)\\&\approx\sum_{n=1}^N\log\Big(\frac{\rho}{N}\sigma_n^2(\mathbf{H})\Big)\\&=N\log\frac{\rho}{N}+\sum_{n=1}^N\log\sigma_n^2(\mathbf{H})\\&=N\log\frac{\rho}{N}+\log\prod_{n=1}^N\sigma_n^2(\mathbf{H})\\&\leq N\log\frac{\rho}{N}+2\log\prod_{n=1}^N\sigma_n(\mathbf{H}_\mathrm{B})\sigma_n(\mathbf{H}_\mathrm{F}),\end{aligned}$$

where the approximation is $\log(1+x)\approx\log(x)$ for large $x$ and the inequality follows from (13a) with $k=N$.

We now show (23) can achieve the upper bounds in (24a) and (24b) simultaneously. On the one hand, (23) is a special case of (15a) with $\mathbf{P}=\mathbf{I}$, which satisfies (16a) and (17a) for $n=1$ and thus attain $\sigma_1(\mathbf{H})=\sigma_1(\mathbf{H}_\mathrm{B})\sigma_1(\mathbf{H}_\mathrm{F})$. On the other hand, since $\log(\cdot)$ is a monotonic function, we can prove similar to Appendix F that $\sum_{n=1}^N\log\sigma_n^2(\mathbf{H})\leq\sum_{n=1}^N\log\sigma_n^2(\mathbf{H}_\mathrm{B})\sigma_n^2(\mathbf{H}_\mathrm{F})$ and the bound is tight at (23). The proof is complete.

## H. Proof of Proposition 4

The sub-differential of a symmetric gauge function of singular values of a matrix with respect to the matrix itself is given by [48, Theorem 2]

$$\partial_{\mathbf{H}^*}f\big(\mathrm{sv}(\mathbf{H})\big)=\mathrm{conv}\big\{\mathbf{U}\mathbf{D}\mathbf{V}^\mathsf{H}\big\}, \quad (58)$$

where $\mathbf{D}\in\mathbb{C}^{N_\mathrm{R}\times N_\mathrm{T}}$ is a rectangular diagonal matrix with $[\mathbf{D}]_{n,n}\in\partial_{\sigma_n(\mathbf{H})}f\big(\mathrm{sv}(\mathbf{H})\big)$, $\forall n\in[N]$, and $\mathbf{U}$, $\mathbf{V}$ are any left and right singular matrices of $\mathbf{H}$. It implies

$$\begin{aligned}\partial f\big(\mathrm{sv}(\mathbf{H})\big)&\ni\mathrm{tr}\big(\mathbf{V}^*\mathbf{D}^\mathsf{T}\mathbf{U}^\mathsf{T}\partial\mathbf{H}^*\big)\\&=\mathrm{tr}\big(\mathbf{V}^*\mathbf{D}^\mathsf{T}\mathbf{U}^\mathsf{T}\mathbf{H}_{\mathrm{B},g}^*\partial\boldsymbol{\Theta}_g^*\mathbf{H}_{\mathrm{F},g}^*\big)\\&=\mathrm{tr}\big(\mathbf{H}_{\mathrm{F},g}^*\mathbf{V}^*\mathbf{D}^\mathsf{T}\mathbf{U}^\mathsf{T}\mathbf{H}_{\mathrm{B},g}^*\partial\boldsymbol{\Theta}_g^*\big),\end{aligned}$$

and therefore $\mathbf{H}_{\mathrm{B},g}^\mathsf{H}\mathbf{U}\mathbf{D}\mathbf{V}^\mathsf{H}\mathbf{H}_{\mathrm{F},g}^\mathsf{H}$ constitutes a sub-gradient of $f\big(\mathrm{sv}(\mathbf{H})\big)$ with respect to $\boldsymbol{\Theta}_g$. The convex hull of those sub-gradients is the sub-differential (26).

## I. Proof of Lemma 1

The differential of $R$ with respect to $\boldsymbol{\Theta}_g^*$ is [63]

$$\partial R=\frac{1}{\eta}\mathrm{tr}\bigg\{\partial\mathbf{H}^*\cdot\mathbf{Q}^\mathsf{T}\mathbf{H}^\mathsf{T}\Big(\mathbf{I}+\frac{\mathbf{H}^*\mathbf{Q}^\mathsf{T}\mathbf{H}^\mathsf{T}}{\eta}\Big)^{-1}\bigg\}$$

$$=\frac{1}{\eta}\mathrm{tr}\left\{\mathbf{H}_{\mathrm{B},g}^{*}\cdot\partial\mathbf{\Theta}_{g}^{*}\cdot\mathbf{H}_{\mathrm{F},g}^{*}\mathbf{Q}^{\mathsf{T}}\mathbf{H}^{\mathsf{T}}\left(\mathbf{I}+\frac{\mathbf{H}^{*}\mathbf{Q}^{\mathsf{T}}\mathbf{H}^{\mathsf{T}}}{\eta}\right)^{-1}\right\}$$
$$=\frac{1}{\eta}\mathrm{tr}\left\{\mathbf{H}_{\mathrm{F},g}^{*}\mathbf{Q}^{\mathsf{T}}\mathbf{H}^{\mathsf{T}}\left(\mathbf{I}+\frac{\mathbf{H}^{*}\mathbf{Q}^{\mathsf{T}}\mathbf{H}^{\mathsf{T}}}{\eta}\right)^{-1}\mathbf{H}_{\mathrm{B},g}^{*}\cdot\partial\mathbf{\Theta}_{g}^{*}\right\},$$

and the corresponding complex derivative is (37).

### J. Proof of Proposition 5

The differential of (39a) with respect to $\mathbf{\Theta}_{g}^{*}$ is

$$\partial\|\mathbf{H}\|_{\mathrm{F}}^{2}=\mathrm{tr}\left(\mathbf{H}_{\mathrm{B},g}^{*}\cdot\partial\mathbf{\Theta}_{g}^{*}\cdot\mathbf{H}_{\mathrm{F},g}^{*}(\mathbf{H}_{\mathrm{D}}^{\mathsf{T}}+\mathbf{H}_{\mathrm{F}}^{\mathsf{T}}\mathbf{\Theta}^{\mathsf{T}}\mathbf{H}_{\mathrm{B}}^{\mathsf{T}})\right)$$
$$=\mathrm{tr}\left(\mathbf{H}_{\mathrm{F},g}^{*}(\mathbf{H}_{\mathrm{D}}^{\mathsf{T}}+\mathbf{H}_{\mathrm{F}}^{\mathsf{T}}\mathbf{\Theta}^{\mathsf{T}}\mathbf{H}_{\mathrm{B}}^{\mathsf{T}})\mathbf{H}_{\mathrm{B},g}^{*}\cdot\partial\mathbf{\Theta}_{g}^{*}\right)$$

and the corresponding complex derivative is

$$\frac{\partial\|\mathbf{H}\|_{\mathrm{F}}^{2}}{\partial\mathbf{\Theta}_{g}^{*}}=\mathbf{H}_{\mathrm{B},g}^{\mathsf{H}}(\mathbf{H}_{\mathrm{D}}+\mathbf{H}_{\mathrm{B}}\mathbf{\Theta}\mathbf{H}_{\mathrm{F}})\mathbf{H}_{\mathrm{F},g}^{\mathsf{H}}\triangleq\mathbf{M}_{g}, \quad (59)$$

whose SVD is denoted as $\mathbf{M}_{g}=\mathbf{U}_{g}\mathbf{\Sigma}_{g}\mathbf{V}_{g}^{\mathsf{H}}$. The quadratic objective (39a) can be successively approximated by its first-order Taylor expansion, resulting in the subproblem

$$\max_{\mathbf{\Theta}} \quad \sum_{g}2\Re\left\{\mathrm{tr}(\mathbf{\Theta}_{g}^{\mathsf{H}}\mathbf{M}_{g})\right\} \quad (60\mathrm{a})$$
$$\mathrm{s.t.} \quad \mathbf{\Theta}_{g}^{\mathsf{H}}\mathbf{\Theta}_{g}=\mathbf{I}, \quad \forall g, \quad (60\mathrm{b})$$

whose optimal solution is

$$\tilde{\mathbf{\Theta}}_{g}=\mathbf{U}_{g}\mathbf{V}_{g}^{\mathsf{H}}, \quad \forall g. \quad (61)$$

This is because $\Re\left\{\mathrm{tr}(\mathbf{\Theta}_{g}^{\mathsf{H}}\mathbf{M}_{g})\right\}=\Re\left\{\mathrm{tr}(\mathbf{\Sigma}_{g}\mathbf{V}_{g}^{\mathsf{H}}\mathbf{\Theta}_{g}^{\mathsf{H}}\mathbf{U}_{g})\right\}\leq \mathrm{tr}(\mathbf{\Sigma}_{g})$ and the bound is tight when $\mathbf{V}_{g}^{\mathsf{H}}\mathbf{\Theta}_{g}^{\mathsf{H}}\mathbf{U}_{g}=\mathbf{I}$.

Next, we prove that solving the affine approximation (60) by (61) does not decrease (39a). Since $\tilde{\mathbf{\Theta}}=\mathrm{diag}(\tilde{\mathbf{\Theta}}_{1},...,\tilde{\mathbf{\Theta}}_{G})$ is optimal for (60), we have

$$2\Re\left\{\sum_{g}\mathrm{tr}(\tilde{\mathbf{\Theta}}_{g}^{\mathsf{H}}\mathbf{H}_{\mathrm{B},g}^{\mathsf{H}}\mathbf{H}_{\mathrm{D}}\mathbf{H}_{\mathrm{F},g}^{\mathsf{H}})\right.$$
$$\left.+\sum_{g_{1},g_{2}}\mathrm{tr}(\tilde{\mathbf{\Theta}}_{g_{1}}^{\mathsf{H}}\mathbf{H}_{\mathrm{B},g_{1}}^{\mathsf{H}}\mathbf{H}_{\mathrm{B},g_{2}}\mathbf{\Theta}_{g_{2}}\mathbf{H}_{\mathrm{F},g_{2}}\mathbf{H}_{\mathrm{F},g_{1}}^{\mathsf{H}})\right\}$$
$$\geq 2\Re\left\{\sum_{g}\mathrm{tr}(\mathbf{\Theta}_{g}^{\mathsf{H}}\mathbf{H}_{\mathrm{B},g}^{\mathsf{H}}\mathbf{H}_{\mathrm{D}}\mathbf{H}_{\mathrm{F},g}^{\mathsf{H}})\right. \quad (62)$$
$$\left.+\sum_{g_{1},g_{2}}\mathrm{tr}(\mathbf{\Theta}_{g_{1}}^{\mathsf{H}}\mathbf{H}_{\mathrm{B},g_{1}}^{\mathsf{H}}\mathbf{H}_{\mathrm{B},g_{2}}\mathbf{\Theta}_{g_{2}}\mathbf{H}_{\mathrm{F},g_{2}}\mathbf{H}_{\mathrm{F},g_{1}}^{\mathsf{H}})\right\}.$$

Besides, $\left\|\sum_{g}\mathbf{H}_{\mathrm{B},g}\tilde{\mathbf{\Theta}}_{g}\mathbf{H}_{\mathrm{F},g}-\sum_{g}\mathbf{H}_{\mathrm{B},g}\mathbf{\Theta}_{g}\mathbf{H}_{\mathrm{F},g}\right\|_{\mathrm{F}}^{2}\geq 0$ implies

$$\sum_{g_{1},g_{2}}\mathrm{tr}(\mathbf{H}_{\mathrm{F},g_{1}}^{\mathsf{H}}\tilde{\mathbf{\Theta}}_{g_{1}}^{\mathsf{H}}\mathbf{H}_{\mathrm{B},g_{1}}^{\mathsf{H}}\mathbf{H}_{\mathrm{B},g_{2}}\tilde{\mathbf{\Theta}}_{g_{2}}\mathbf{H}_{\mathrm{F},g_{2}})$$
$$+\sum_{g_{1},g_{2}}\mathrm{tr}(\mathbf{H}_{\mathrm{F},g_{1}}^{\mathsf{H}}\mathbf{\Theta}_{g_{1}}^{\mathsf{H}}\mathbf{H}_{\mathrm{B},g_{1}}^{\mathsf{H}}\mathbf{H}_{\mathrm{B},g_{2}}\mathbf{\Theta}_{g_{2}}\mathbf{H}_{\mathrm{F},g_{2}}) \quad (63)$$
$$\geq 2\Re\left\{\sum_{g_{1},g_{2}}\mathrm{tr}(\mathbf{H}_{\mathrm{F},g_{1}}^{\mathsf{H}}\tilde{\mathbf{\Theta}}_{g_{1}}^{\mathsf{H}}\mathbf{H}_{\mathrm{B},g_{1}}^{\mathsf{H}}\mathbf{H}_{\mathrm{B},g_{2}}\mathbf{\Theta}_{g_{2}}\mathbf{H}_{\mathrm{F},g_{2}})\right\}.$$

Adding (62) and (63), we have

$$2\Re\left\{\mathrm{tr}(\tilde{\mathbf{\Theta}}^{\mathsf{H}}\mathbf{H}_{\mathrm{B}}^{\mathsf{H}}\mathbf{H}_{\mathrm{D}}\mathbf{H}_{\mathrm{F}}^{\mathsf{H}})\right\}+\mathrm{tr}(\mathbf{H}_{\mathrm{F}}^{\mathsf{H}}\tilde{\mathbf{\Theta}}^{\mathsf{H}}\mathbf{H}_{\mathrm{B}}^{\mathsf{H}}\mathbf{H}_{\mathrm{B}}\tilde{\mathbf{\Theta}}\mathbf{H}_{\mathrm{F}})$$
$$\geq 2\Re\left\{\mathrm{tr}(\mathbf{\Theta}^{\mathsf{H}}\mathbf{H}_{\mathrm{B}}^{\mathsf{H}}\mathbf{H}_{\mathrm{D}}\mathbf{H}_{\mathrm{F}}^{\mathsf{H}})\right\}+\mathrm{tr}(\mathbf{H}_{\mathrm{F}}^{\mathsf{H}}\mathbf{\Theta}^{\mathsf{H}}\mathbf{H}_{\mathrm{B}}^{\mathsf{H}}\mathbf{H}_{\mathrm{B}}\mathbf{\Theta}\mathbf{H}_{\mathrm{F}}), \quad (64)$$

which suggests that (39a) is non-decreasing as the solution iterates over (61). Since (39a) is also bounded from above, the sequence of objective value converges.

Finally, we prove that any solution when (40) converges, denoted by $\mathbf{\Theta}'$, is a stationary point of (39). The Karush-Kuhn-Tucker (KKT) conditions of (39) and (60) are equivalent in terms of primal/dual feasibility and complementary slackness, while the stationary conditions are respectively, $\forall g$,

$$\mathbf{H}_{\mathrm{B},g}^{\mathsf{H}}(\mathbf{H}_{\mathrm{D}}+\mathbf{H}_{\mathrm{B}}\mathbf{\Theta}^{\star}\mathbf{H}_{\mathrm{F}})\mathbf{H}_{\mathrm{F},g}^{\mathsf{H}}-\mathbf{\Theta}_{g}^{\star}\mathbf{\Lambda}_{g}^{\mathsf{H}}=0, \quad (65)$$
$$\mathbf{M}_{g}-\mathbf{\Theta}_{g}^{\star}\mathbf{\Lambda}_{g}^{\mathsf{H}}=0. \quad (66)$$

When (40) converges, $\mathbf{H}_{\mathrm{B},g}^{\mathsf{H}}(\mathbf{H}_{\mathrm{D}}+\mathbf{H}_{\mathrm{B}}\mathbf{\Theta}'\mathbf{H}_{\mathrm{F}})\mathbf{H}_{\mathrm{F},g}^{\mathsf{H}}=\mathbf{H}_{\mathrm{B},g}^{\mathsf{H}}(\mathbf{H}_{\mathrm{D}}+\mathbf{H}_{\mathrm{B}}\mathbf{\Theta}^{\star}\mathbf{H}_{\mathrm{F}})\mathbf{H}_{\mathrm{F},g}^{\mathsf{H}}$ and (66) reduces to (65). The proof is thus completed.

### REFERENCES

[1] E. Basar, M. D. Renzo, J. D. Rosny, M. Debbah, M.-S. Alouini, and R. Zhang, "Wireless communications through reconfigurable intelligent surfaces," *IEEE Access*, vol. 7, pp. 116 753–116 773, 2019.

[2] Q. Wu and R. Zhang, "Intelligent reflecting surface enhanced wireless network via joint active and passive beamforming," *IEEE Transactions on Wireless Communications*, vol. 18, pp. 5394–5409, Nov 2019.

[3] H. Guo, Y.-C. Liang, J. Chen, and E. G. Larsson, "Weighted sum-rate maximization for reconfigurable intelligent surface aided wireless networks," *IEEE Transactions on Wireless Communications*, vol. 19, pp. 3064–3076, May 2020.

[4] Y. Liu, Y. Zhang, X. Zhao, S. Geng, P. Qin, and Z. Zhou, "Dynamic-controlled RIS assisted multi-user MISO downlink system: Joint beamforming design," *IEEE Transactions on Green Communications and Networking*, vol. 6, pp. 1069–1081, Jun 2022.

[5] Y. He, Y. Cai, H. Mao, and G. Yu, "RIS-assisted communication radar coexistence: Joint beamforming design and analysis," *IEEE Journal on Selected Areas in Communications*, vol. 40, pp. 2131–2145, Jul 2022.

[6] H. Luo, R. Liu, M. Li, Y. Liu, and Q. Liu, "Joint beamforming design for RIS-assisted integrated sensing and communication systems," *IEEE Transactions on Vehicular Technology*, vol. 71, pp. 13 393–13 397, Dec 2022.

[7] M. Hua, Q. Wu, C. He, S. Ma, and W. Chen, "Joint active and passive beamforming design for IRS-aided radar-communication," *IEEE Transactions on Wireless Communications*, vol. 22, pp. 2278–2294, Apr 2023.

[8] Q. Wu and R. Zhang, "Joint active and passive beamforming optimization for intelligent reflecting surface assisted SWIPT under QoS constraints," *IEEE Journal on Selected Areas in Communications*, vol. 38, no. 8, pp. 1735–1748, Aug 2020.

[9] Z. Feng, B. Clerckx, and Y. Zhao, "Waveform and beamforming design for intelligent reflecting surface aided wireless power transfer: Single-user and multi-user solutions," *IEEE Transactions on Wireless Communications*, 2022.

[10] Y. Zhao, B. Clerckx, and Z. Feng, "IRS-aided SWIPT: Joint waveform, active and passive beamforming design under nonlinear harvester model," *IEEE Transactions on Communications*, vol. 70, pp. 1345–1359, 2022.

[11] R. Karasik, O. Simeone, M. D. Renzo, and S. S. Shitz, "Beyond max-SNR: Joint encoding for reconfigurable intelligent surfaces," in *2020 IEEE International Symposium on Information Theory (ISIT)*, Jun 2020, pp. 2965–2970.

[12] J. Ye, S. Guo, S. Dang, B. Shihada, and M.-S. Alouini, "On the capacity of reconfigurable intelligent surface assisted MIMO symbiotic communications," *IEEE Transactions on Wireless Communications*, vol. 21, pp. 1943–1959, Mar 2022.

[13] Y.-C. Liang, Q. Zhang, E. G. Larsson, and G. Y. Li, "Symbiotic radio: Cognitive backscattering communications for future wireless networks," *IEEE Transactions on Cognitive Communications and Networking*, vol. 6, pp. 1242–1255, Dec 2020.

[14] Y. Zhao and B. Clerckx, "RIScatter: Unifying backscatter communication and reconfigurable intelligent surface," *IEEE Journal on Selected Areas in Communications*, pp. 1–1, Dec 2024.

[15] E. Basar, "Reconfigurable intelligent surfaces for doppler effect and multipath fading mitigation," *Frontiers in Communications and Networks*, vol. 2, May 2021.

[16] E. Arslan, I. Yildirim, F. Kilinc, and E. Basar, "Over-the-air equalization with reconfigurable intelligent surfaces," *IET Communications*, vol. 16, pp. 1486–1497, Aug 2022.

[17] O. Ozdogan, E. Bjornson, and E. G. Larsson, "Using intelligent reflecting surfaces for rank improvement in MIMO communications," in *ICASSP 2020 - 2020 IEEE International Conference on Acoustics, Speech and Signal Processing (ICASSP)*, May 2020, pp. 9160–9164.

[18] Y. Yang, B. Zheng, S. Zhang, and R. Zhang, "Intelligent reflecting surface meets OFDM: Protocol design and rate maximization," *IEEE Transactions on Communications*, vol. 68, pp. 4522–4535, Jul 2020.

[19] G. Chen and Q. Wu, "Fundamental limits of intelligent reflecting surface aided multiuser broadcast channel," *IEEE Transactions on Communications*, vol. 71, pp. 5904–5919, Oct 2023.

[20] M. A. ElMossallamy, H. Zhang, R. Sultan, K. G. Seddik, L. Song, G. Y. Li, and Z. Han, "On spatial multiplexing using reconfigurable intelligent surfaces," *IEEE Wireless Communications Letters*, vol. 10, pp. 226–230, Feb 2021.

[21] S. Meng, W. Tang, W. Chen, J. Lan, Q. Y. Zhou, Y. Han, X. Li, and S. Jin, "Rank optimization for MIMO channel with RIS: Simulation and measurement," *IEEE Wireless Communications Letters*, vol. 13, pp. 437–441, Feb 2024.

[22] W. Huang, B. Lei, S. He, C. Kai, and C. Li, "Condition number improvement of IRS-aided near-field MIMO channels," in *2023 IEEE International Conference on Communications Workshops (ICC Workshops)*, May 2023, pp. 1210–1215.

[23] S. H. Chae and K. Lee, "Cooperative communication for the rank-deficient MIMO interference channel with a reconfigurable intelligent surface," *IEEE Transactions on Wireless Communications*, vol. 22, pp. 2099–2112, Mar 2023.

[24] S. Shen and B. Clerckx, "Beamforming optimization for MIMO wireless power transfer with nonlinear energy harvesting: RF combining versus DC combining," *IEEE Transactions on Wireless Communications*, vol. 20, pp. 199–213, Jan 2021.

[25] S. Shen, B. Clerckx, and R. Murch, "Modeling and architecture design of reconfigurable intelligent surfaces using scattering parameter network analysis," *IEEE Transactions on Wireless Communications*, vol. 21, pp. 1229–1243, Feb 2022.

[26] M. Nerini, S. Shen, and B. Clerckx, "Closed-form global optimization of beyond diagonal reconfigurable intelligent surfaces," *IEEE Transactions on Wireless Communications*, vol. 23, pp. 1037–1051, Feb 2024.

[27] M. Nerini, S. Shen, H. Li, and B. Clerckx, "Beyond diagonal reconfigurable intelligent surfaces utilizing graph theory: Modeling, architecture design, and optimization," *IEEE Transactions on Wireless Communications*, pp. 1–1, May 2024.

[28] I. Santamaria, M. Soleymani, E. Jorswieck, and J. Gutiérrez, "SNR maximization in beyond diagonal RIS-assisted single and multiple antenna links," *IEEE Signal Processing Letters*, vol. 30, pp. 923–926, 2023.

[29] ——, "Interference leakage minimization in RIS-assisted MIMO interference channels," in *ICASSP 2023 - 2023 IEEE International Conference on Acoustics, Speech and Signal Processing (ICASSP)*, vol. 39, Jun 2023, pp. 1–5.

[30] H.-R. Ahn, *Asymmetric Passive Components in Microwave Integrated Circuits*. Hoboken, NJ, USA: Wiley, 2006.

[31] H. Li, S. Shen, and B. Clerckx, "Beyond diagonal reconfigurable intelligent surfaces: A multi-sector mode enabling highly directional full-space wireless coverage," *IEEE Journal on Selected Areas in Communications*, vol. 41, pp. 2446–2460, Aug 2023.

[32] H. Li, S. Shen, Y. Zhang, and B. Clerckx, "Channel estimation and beamforming for beyond diagonal reconfigurable intelligent surfaces," *IEEE Transactions on Signal Processing*, vol. 72, pp. 3318–3332, Jan 2024.

[33] H. Li, S. Shen, M. Nerini, M. D. Renzo, and B. Clerckx, "Beyond diagonal reconfigurable intelligent surfaces with mutual coupling: Modeling and optimization," *IEEE Communications Letters*, pp. 1–1, Oct 2024.

[34] H. Li, M. Nerini, S. Shen, and B. Clerckx, "Wideband modeling and beamforming for beyond diagonal reconfigurable intelligent surfaces," in *2024 IEEE 25th International Workshop on Signal Processing Advances in Wireless Communications (SPAWC)*, Jun 2024, pp. 926–930.

[35] T. Fang and Y. Mao, "A low-complexity beamforming design for beyond-diagonal RIS aided multi-user networks," *IEEE Communications Letters*, pp. 1–1, Jul 2023.

[36] Y. Zhou, Y. Liu, H. Li, Q. Wu, S. Shen, and B. Clerckx, "Optimizing power consumption, energy efficiency and sum-rate using beyond diagonal RIS — a unified approach," *IEEE Transactions on Wireless Communications*, pp. 1–1, 2023.

[37] G. Bartoli, A. Abrardo, N. Decarli, D. Dardari, and M. D. Renzo, "Spatial multiplexing in near field MIMO channels with reconfigurable intelligent surfaces," *IET Signal Processing*, vol. 17, Mar 2023.

[38] A. Mishra, Y. Mao, C. D'Andrea, S. Buzzi, and B. Clerckx, "Transmitter side beyond-diagonal reconfigurable intelligent surface for massive MIMO networks," *IEEE Wireless Communications Letters*, vol. 13, pp. 352–356, Feb 2024.

[39] M. Nerini, S. Shen, and B. Clerckx, "Discrete-value group and fully connected architectures for beyond diagonal reconfigurable intelligent surfaces," *IEEE Transactions on Vehicular Technology*, vol. 72, pp. 16 354–16 368, Dec 2023.

[40] D. Semmler, M. Joham, and W. Utschick, "High SNR analysis of RIS-aided MIMO broadcast channels," in *2023 IEEE 24th International Workshop on Signal Processing Advances in Wireless Communications (SPAWC)*, Sep 2023, pp. 221–225.

[41] L. Hogben, Ed., *Handbook of Linear Algebra*. Boca Raton, FL, USA: CRC press, 2013.

[42] R. A. Horn and C. R. Johnson, *Topics in Matrix Analysis*. Cambridge, UK: Cambridge University Press, Jun 1994.

[43] W. Fulton, "Eigenvalues, invariant factors, highest weights, and schubert calculus," *Bulletin of the American Mathematical Society*, vol. 37, pp. 209–249, Apr 2000.

[44] R. Bhatia, "Linear algebra to quantum cohomology: The story of alfred horn's inequalities," *The American Mathematical Monthly*, vol. 108, pp. 289–318, Apr 2001.

[45] Y. Rong and Y. Hua, "Optimality of diagonalization of multi-hop MIMO relays," *IEEE Transactions on Wireless Communications*, vol. 8, no. 12, pp. 6068–6077, Dec 2009.

[46] A. Zanella, M. Chiani, and M. Win, "On the marginal distribution of the eigenvalues of wishart matrices," *IEEE Transactions on Communications*, vol. 57, pp. 1050–1060, Apr 2009.

[47] B. Clerckx and C. Oestges, *MIMO Wireless Networks: Channels, Techniques and Standards for Multi-Antenna, Multi-User and Multi-Cell Systems*. Waltham, MA, USA: Academic Press, 2013.

[48] G. A. Watson, "Characterization of the subdifferential of some matrix norms," *Linear Algebra and its Applications*, vol. 170, no. 1, pp. 33–45, 1992.

[49] T. E. Abrudan, J. Eriksson, and V. Koivunen, "Steepest descent algorithms for optimization under unitary matrix constraint," *IEEE Transactions on Signal Processing*, vol. 56, pp. 1134–1147, Mar 2008.

[50] T. Abrudan, J. Eriksson, and V. Koivunen, "Conjugate gradient algorithm for optimization under unitary matrix constraint," *Signal Processing*, vol. 89, pp. 1704–1714, Sep 2009.

[51] W. W. Hager and H. Zhang, "A survey of nonlinear conjugate gradient methods," *Pacific journal of Optimization*, vol. 2, 2006.

[52] L. Armijo, "Minimization of functions having lipschitz continuous first partial derivatives," *Pacific Journal of Mathematics*, vol. 16, pp. 1–3, Jan 1966.

[53] C. Moler and C. V. Loan, "Nineteen dubious ways to compute the exponential of a matrix, twenty-five years later," *SIAM Review*, vol. 45, pp. 3–49, Jan 2003.

[54] F. Liu, Y. Cui, C. Masouros, J. Xu, T. X. Han, Y. C. Eldar, and S. Buzzi, "Integrated sensing and communications: Toward dual-functional wireless networks for 6G and beyond," *IEEE Journal on Selected Areas in Communications*, vol. 40, pp. 1728–1767, Jun 2022.

[55] F. Nie, R. Zhang, and X. Li, "A generalized power iteration method for solving quadratic problem on the Stiefel manifold," *Science China Information Sciences*, vol. 60, p. 112101, Nov 2017.

[56] J. H. Manton, "Optimization algorithms exploiting unitary constraints," *IEEE Transactions on Signal Processing*, vol. 50, pp. 635–650, Mar 2002.

[57] T. Viklands, "Algorithms for the weighted orthogonal procrustes problem and other least squares problems," PhD dissertation, Datavetenskap, Umeå University, 2006.

[58] T. Bell, "Global positioning system-based attitude determination and the orthogonal procrustes problem," *Journal of Guidance, Control, and Dynamics*, vol. 26, pp. 820–822, Sep 2003.

[59] G. H. Golub and C. F. V. Loan, *Matrix Computations*. Baltimore, MD, USA: Johns Hopkins University Press, 2013.

[60] K. D. Ikramov, "Takagi's decomposition of a symmetric unitary matrix as a finite algorithm," *Computational Mathematics and Mathematical Physics*, vol. 52, pp. 1–3, Jan 2012.

[61] F. Zhang, Ed., *The Schur Complement and Its Applications*, ser. Numerical Methods and Algorithms. New York, NY, USA: Springer, Apr 2005.

[62] A. W. Marshall, I. Olkin, and B. C. Arnold, *Inequalities: Theory of Majorization and Its Applications*, 2nd ed., ser. Springer Series in Statistics. New York, NY, USA: Springer, Dec 2010.

[63] A. Hjorungnes and D. Gesbert, "Complex-valued matrix differentiation: Techniques and key results," *IEEE Transactions on Signal Processing*, vol. 55, pp. 2740–2746, Jun 2007.